Human Hsp70 disaggregase reverses Parkinson's-linked α-synuclein amyloid fibrils

Xuechao Gao[1], Marta Carroni[2], Carmen Nussbaum-Krammer[1], Axel Mogk[1], Nadinath B. Nillegoda[1], Anna Szlachcic[1], D. Lys Guilbride[3], Helen R. Saibil[2], Matthias P. Mayer[3] and Bernd Bukau[1*]

[1] Center for Molecular Biology of the University of Heidelberg (ZMBH) and German Cancer Research Center (DKFZ), DKFZ-ZMBH Alliance, Im Neuenheimer Feld 282, D-69120 Heidelberg, Germany
[2] Department of Crystallography, Institute for Structural and Molecular Biology, Birkbeck College, Malet Street, London WC1E 7HX, United Kingdom.
[3] ZMBH, DKFZ-ZMBH Alliance, Im Neuenheimer Feld 282, D-69120 Heidelberg, Germany

* Corresponding author: bukau@zmbh.uni-heidelberg.de
phone: +49 6221 54 6795

Key words:
Hsp70, Hsp110, chaperones, amyloid fibril, disaggregation, Parkinson's disease, α-synuclein, proteostasis

Highlights:

- Specific human Hsp70 chaperone system efficiently disassembles α-synuclein fibrils.
- Fragmentation and depolymerisation generate short fibrils and non-toxic monomers.
- Coordinated chaperone binding cycles generate power stroke for disassembly.
- Fibril disassembly requires N- and C-terminal α-synuclein extensions.

Abstract

Intracellular amyloid fibrils linked to neurodegenerative disease typically accumulate in an age-dependent process, suggesting an inherent cellular capacity for counteracting amyloid formation in early life. Molecular chaperones assist native folding and block polymerization of amyloidogenic proteins, preempting amyloid fibril formation. The capacity of metazoan chaperones for amyloid disassembly, however, is unclear. Here, we show a specific combination of human Hsp70 chaperone components efficiently disassembles α-synuclein amyloid fibrils, characteristic of Parkinson's disease, *in vitro.* Specifically, the Hsc70 chaperone, the class B J-protein DNAJB1 and an Hsp110-family nucleotide exchange factor (NEF) provide an ATP-dependent activity that disassembles amyloids within minutes via combined fibril fragmentation and depolymerisation, ultimately generating non-toxic α-synuclein monomers. Concerted, rapid interaction cycles of all three chaperone components with fibrils generate the power stroke required for disassembly. This identifies a powerful human Hsp70 disaggregase activity that efficiently disassembles amyloid fibrils and a mammalian protein quality control pathway crucial to the biology of amyloid-based neurodegenerative diseases.

Introduction

Many neurodegenerative diseases are characterized by the misfolding and oligomerisation of specific proteins, leading to amyloid-type fibril formation. Examples include α-synuclein (α-Syn) in Parkinson's disease, β-amyloid (Aβ) and Tau in Alzheimer's disease and tauopathies, superoxide dismutase (SOD1) in amyotrophic lateral sclerosis and polyglutamine-expanded huntingtin in Huntington's disease (Knowles et al., 2014). Typically, these diseases are of late-onset, but the factors determining oligomerisation and fibril formation in cells are poorly defined. Even in mutation-driven manifestations, the toxicity-generating protein remains latent for years, often decades, before clinical or microscopic symptoms are detectable (Blennow et al., 2006). Increasing evidence pinpoints oligomeric, shorter forms as the

more neurotoxic conformers of amyloidogenic proteins, but amyloid fibrils can also exhibit cell toxicity (Bieschke et al., 2010; Caughey and Lansbury, 2003; Dedmon et al., 2005; Pieri et al., 2012).

Oligomerisation and fibril formation depend on rate-limiting conformational alterations of the amyloidogenic proteins and generation of fibril-nucleating oligomers (Jarrett and Lansbury, 1993; Lomakin et al., 1996), and are counteracted by cellular protein quality surveillance activities. In quality control, molecular chaperones recognize misfolded proteins and respond either by targeting them for degradation (Kim et al., 2013) or, via "holdase" function, stabilizing folding intermediates to favor refolding to the native state, preempting fibril formation. A range of different metazoan chaperones and co-chaperones including Hsp70, J-domain proteins (J-proteins), Hsp110 and small HSPs associate with α-Syn and other amyloidogenic proteins in various oligomeric states (Cantuti-Castelvetri et al., 2005; Chen et al., 2011; Wang et al., 2009). These are known to suppress amyloid fibril formation both *in vivo* (Kieran et al., 2004; Takeuchi et al., 2002) and *in vitro* (Dedmon et al., 2005; Evans et al., 2006; Huang et al., 2006; Lee et al., 2005; Muchowski and Wacker, 2005) via holdase function. Whether metazoan chaperones can directly disintegrate already existing fibrils however, is less clear. Chaperone-mediated amyloid disassembly would immediately impact pathophysiology, by affecting levels of amyloids and oligomeric species linked to cell toxicity.

In yeast cells, fibrils are fragmented by the powerful bi-chaperone system consisting of the AAA+ Hsp100 disaggregase and the Hsp70 chaperone and its J-protein co-chaperone (Helsen and Glover, 2012; Higurashi et al., 2008; Reidy et al., 2012; Shorter and Lindquist, 2004; Tuite et al., 2011; Winkler et al., 2012). Metazoans, however, entirely lack the Hsp100 family disaggregases in the cytosol and nucleus, and efficient *in vitro* disassembly of metazoan amyloid aggregates on a physiologically relevant time scale (minutes to hours), has so far not been demonstrated (Bieschke et al., 2009; Duennwald et al., 2012; Evans et al., 2006; Murray et al., 2013; Murray et al., 2010). Metazoans do nonetheless solubilize amorphous, stress-induced protein aggregates, both *in vivo* and *in vitro*. Disaggregation of amorphous aggregates, which are considered to be energetically less stable

than amyloid fibrils, is provided by Hsp70 chaperones together with co-chaperones of the J-protein family and Hsp110 nucleotide exchange factors (NEFs) (Rampelt et al., 2012; Shorter, 2011). J-proteins bind substrates and stimulate ATP hydrolysis by Hsp70, which traps substrates in complex with Hsp70. NEFs then stimulate ADP release enabling rebinding of ATP to Hsp70 with concomitant substrate release (Bukau and Horwich, 1998). However, when tested for its ability to disassemble amyloids *in vitro,* the human Hsp70 machinery disassembled α-Syn amyloids only extremely slowly, at a time scale of weeks (Duennwald et al., 2012). The efficacy, and hence pathophysiological relevance, of cellular amyloid disaggregation activity therefore remains a largely unsolved issue.

We therefore investigated in detail the potential of the human Hsp70 network for α-Syn amyloid disassembly. Here, we examine the interaction of a variety of constituents of the Hsp70 machinery with α-Syn amyloid fibrils preformed *in vitro*. We find that the constitutively expressed Hsc70 (HSPA8), the class B J-protein DNAJB1, and the Hsp110-family NEFs Apg2 or Hsp105, form a specific, surprisingly powerful ATP-driven metazoan disaggregase for amyloids, that efficiently disassembles α-Syn fibrils *in vitro*. The disaggregase activity fragments α-Syn fibrils into increasingly shorter fibrils and promotes depolymerisation into non-toxic α-Syn monomers within minutes. We directly visualize and dissect the kinetics of chaperone association with α-Syn fibrils and fibril disintegration by electron microscopy (EM) combined with biochemical and fluorescence techniques. Our findings provide the basis for a model of chaperone function in amyloid fibril disassembly.

Results

A human Hsp70 disaggregase solubilizes α-Syn fibrils in vitro

We initially tested several different major components of the human cytosolic Hsp70 chaperone system, individually and in combination, for α-Syn fibril disassembly activity. For disassembly assays we used established Hsp70-based protein disaggregation reaction conditions (Dragovic et al., 2006; Rampelt et al., 2012; Tzankov et al., 2008) and a homogeneous substrate of

preformed α-Syn amyloid fibrils, verified by negative stain transmission EM (Figure 1A). We analyzed solubilized reaction products, separated by centrifugation and identified by SDS-PAGE and immunoblotting with an α-Syn-specific antibody. Individually, the constitutively expressed chaperone Hsc70 (HSPA8), the heat-inducible chaperone Hsp70 (HSPA1A), the J-protein co-chaperones of classes A (Hdj2; DNAJA1) and B (Hdj1; DNAJB1), and the Hsp110-family NEF Apg2 (HSPA4; HSPH2) are unable to solubilize α-Syn from preformed fibrils. Hsc70 in combination with DNAJB1 solubilizes only a small fraction of the α-syn fibril material (Figure 1B). However, with the addition of either Hsp110-family NEF Apg2 or Hsp105α into the reaction containing Hsc70 and DNAJB1, solubilization increases dramatically in an ATP-dependent manner (Figures 1B and S1A). An alternative, Bag family type NEF (Bag1), is only about 20% as efficient (Figure S1A), which demonstrates high selectivity for the effective NEF. Under these conditions, DNAJB1-Agp2 combinations containing Hsc70 solubilize fibrils to greater extent than combinations containing stress-inducible Hsp70 (Figure S1A). Also, the Hsc70-Agp2 combination showed activity only in combination with class B J-protein DNAJB1 and not with class A DNAJA1 (Figure S1A). We infer the Hsc70–DNAJB1-Hsp110 machinery has highly efficient disaggregation activity on α-Syn fibrils. This basic combination of chaperones is therefore used for all further experiments, unless otherwise indicated.

Complete fibril solubilization occurs with fast kinetics

A ratio of chaperones (Hsc70/DNAJB1/Apg2) to α-Syn of 1:1 (Hsc70:α-Syn monomer) converts 50% of fibrillar α-Syn (at 2 μM α-Syn monomer concentration) to soluble material within 8 h (Figure 1C). Higher relative amounts of the machinery compared to fibrils (Hsc70:α-Syn of 2:1 and 5:1), with Hsc70:DNAJB1:Apg2 stoichiometries kept constant at 1:0.5:0.1, work dramatically faster. At 5:1 Hsc70:α-Syn ratio, the chaperone combination converts 50% of α-Syn fibrils to soluble form within 40 min (Figure 1C). Yields of solubilized fibrils are maximally 70-80% of total α-Syn, at all ratios tested. This maximum may be due to exhaustion of the chaperone machinery during the 24 h incubation time (e.g. by chaperone aggregation, drop in ATP levels,

absorption to the test tube). This is supported by experiments described below, where successive addition of chaperones allows for continued fibril disassembly (Figure S3B). We infer that the human Hsc70 chaperone-co-chaperone system can, in principle, solubilize α-Syn amyloid fibrils to completion. Further, the *in vitro* reaction occurs within minutes at 30°C, implying that under the physiological temperature for human cells (37°C) disassembly is likely to be at least as efficient. The concentration of Hsc70 monomers in human cells is around 10 μM (Nollen et al., 2000), and estimated to be 2500-fold higher than that of α-Syn monomers in various human cell types (Finka and Goloubinoff, 2013). This suggests the concentrations required for efficient fibril disassembly *in vitro* are in principle attainable in cells. For instance at the 1:1 Hsc70:α-Syn ratio used in our assays, the Hsc70 concentration is 2 μM, which is well within the physiological concentration range.

We then examined the α-Syn species solubilized after 4 h incubation with Hsc70/DNAJB1/Apg2. We distinguished monomeric α-Syn from small oligomeric products using a fluorescence assay. We formed fibrils from a cysteine variant of α-Syn (α-Syn-S9C) that have indistinguishable morphology by EM from fibrils formed of wild-type α-Syn (Figure S1B). Labeling of the fibrils with the thiol-specific fluorescent dye Alexa488-maleimide (Alexa488-α-Syn) allows sensitive fluorescence detection of solubilized species by gel filtration. Most soluble material (>80%) eluted with monomeric α-Syn (Figures 1D and 1E). Since the dye fluorescence is quenched by incorporation into the α-Syn fibrils (Graf et al., 2009; Kityk et al., 2012), we also followed fibril disassembly by fluorescence dequenching in real time (Figure S1C). Dequenching depends strictly on the presence of Hsc70/DNAJB1 and ATP, and is greatly accelerated by Apg2. The addition of Bag1 instead of Apg2 leads to much less dequenching (approx. 80% less). We conclude specific compositions of the human Hsc70 chaperone system constitute a powerful ATP-driven disaggregase capable of extensively solubilizing α-Syn fibrils to monomers.

The human Hsp70 system solubilizes α-Syn aggregates generated in vivo

To determine whether Hsc70/DNAJB1/Apg2 will also disassemble α-Syn aggregates produced *in vivo*, we overexpressed human α-Syn fused to YFP in *Caenorhabditis elegans* muscle cells (van Ham et al., 2008). Detergent (1% Sarkosyl)-resistant α-Syn aggregates were isolated. Upon 4 h incubation with the human Hsc70/DNAJB1/Apg2 chaperone system and ATP, α-Syn-YFP shifted partially from the pellet to the supernatant fraction after centrifugation (Figure 1F). We infer α-Syn aggregates preformed *in vivo* are efficiently disassembled.

Dual mechanism of fibril disassembly

Two non-exclusive molecular mechanisms accommodate Hsc70-based α-Syn fibril disassembly. A fragmentation activity similar to that of the Hsp100 disaggregase on yeast Sup35 and Ure2 prions (Inoue and Yoshida, 2006; Shorter and Lindquist, 2006) may break fibrils into shorter fragments and finally to monomers. Alternatively, depolymerization by dissociation of single α-Syn molecules from fibril ends (and perhaps internal sites of fibrils) may also drive solubilization of fibrils to monomers. We employed three approaches to investigate these two mechanisms.

In a first approach we estimated the lengths of 600 chaperone-treated and untreated α-Syn fibrils from 64 randomly chosen representative EM pictures per reaction time point (Figure S2A shows representative EM pictures). Depolymerization alone might be expected to decrease length at a similar rate in all fibrils, accompanied by corresponding increase in soluble monomeric α-Syn. The average mature fibril length was approximately 1000 nm (Figure 2A). In control reactions lacking chaperones, fibril length distribution did not change over time. In the presence of Hsc70/DNAJB1/Apg2 and ATP, the longer fibrils (>500 nm length) decreased rapidly in number, the longest fibrils (>2000 nm) disappearing even within 2 min (Figures 2A and S2A). In contrast, short fibrils (<500 nm) increased in abundance over the entire 24 h incubation time, which is incompatible with a depolymerisation-only mechanism. Furthermore, fibril shortening by depolymerization alone would require a very high initial depolymerization rate during the noticeably fast first 2 min of reaction, and would result in substantial solubilized monomeric material. We did not see this (Figure 1C, inset). We infer

fragmentation, rather than depolymerization, contributes most significantly to initial fibril shortening.

A second approach directly detects fibril fragmentation. We used preformed α-Syn fibrils capped with biotinylated Avi-tagged α-Syn (Beckett et al., 1999). This allows fibrils to bind streptavidin-coated magnetic beads (Figure 2B), which enables magnetic separation from released material after incubation with chaperones, a method successfully used for yeast prions (Inoue and Yoshida, 2006). Analyses by SDS-PAGE, native PAGE and EM show ATP and chaperone dependent release of wild-type α-Syn, but not biotinylated Avi-tagged α-Syn from the capped fibrils (Figure 2C). After 2 h of treatment with the complete chaperone system about 20% of bound α-Syn was released (Figures 2C and S2B). Three cycles of newly added chaperones released additional α-Syn, to a total of 60% of input (Figure S2C). Native PAGE reveals a mixture of monomeric and oligomeric α-Syn species in the released material (Figure S2D). EM images of this released material show short fibrils with a significantly shorter average length than that of untreated capped α-Syn fibrils. We infer that chaperone action promotes fibril depolymerisation as well as fragmentation (Figure 2D).

A third approach further characterizes fibril disassembly by fractionating reaction products using density gradient centrifugation (Figure 3A). Monomeric α-Syn appears prominently in fractions 1-4; mature fibrils pellet in fraction 25. After 2 min incubation with Hsc70/DNAJB1/Apg2 and ATP, α-Syn was detected in fractions 1-4, 10-19, and 25 but not in fractions 5-9 and 20-24. EM images show quantity of fibrils peaking in fractions 10-19. These are on average shorter than fibrils in fraction 25 (Figure 3B). Control reactions with incomplete chaperone combinations detect α-Syn mainly in fraction 25 that is, in intact fibril form (Figure S3A). Efficient fibril shortening therefore requires the full chaperone system. We further infer that mature fibrils do not shorten gradually but are cut into shorter fragments of intermediate length. With increasing incubation time, the amount of mature α-Syn fibrils in fraction 25 decreases rapidly. In contrast, amounts of shortened fibrils from intermediate fractions (10-19 pool II) initially (after 30 min reaction) increased, but then (after 2 h) decreased. The position of peak fractions of shortened fibril does not shift during the incubation time (Figure S3B).

However, the amounts of α-Syn in fractions 1-4 (pool I) increased continuously and most dramatically after 2 h (Figure 3C). This suggests rapid conversion of short fibrils to monomers as the reaction proceeds. The increase of monomeric α-Syn is non-linear on a logarithmic timescale (Figure 3C) and correlates with the gradual increase in number of fibril ends over time. We do not detect α-Syn in fractions 5 to 9 by immunoblot analysis, suggesting that disassembly of the short fibrils is very rapid, and may involve an efficient depolymerisation mechanism.

A disaggregation mechanism involving depolymerisation is further supported by quantitative assessment of the experimental data. After 50 min of reaction, approximately 50% of the total input of α-Syn protomers is converted to intermediate fibrils (middle fractions 10-19) and 25% appears in monomer fractions (Figure 3C). Based on the average length of the short fibrils (254 nm) and the protomer arrangement in the structural model of α-Syn fibrils (Vilar et al., 2008) (see Experimental procedures for details) we estimate that short fibrils consist of, on average, 2000 α-Syn protomers. The molar ratio of short fibrils to monomers is thus approximately 1:1000 (0.5/2000:0.25/1) after 50 min of reaction. Monomeric α-Syn therefore, cannot be the sole immediate byproduct of the fragmentation action of Hsc70/DNAJB1/Apg2. We infer from this high ratio of monomer to fragment that most monomeric α-Syn is produced by end-depolymerization.

EM analysis of fibril disintegration

We investigated the molecular features of the fibril disintegration process by electron microscopy. Inspection of fractionated reaction samples containing shortened fibrils (fraction 15) by negative stain EM shows these are frequently coated with large and amorphous globular structures (Figure 3D) exceeding the size observed for chaperones associated with fibrils. These structures probably represent small α-Syn oligomers originally disassembled from mature fibrils. In many images short fibrils appear aligned (Figures 3D and S3E). This is not seen in untreated samples, nor in samples incubated with an incomplete complement of chaperone machinery (Figure S3E). We surmise the short fibril alignment results from the severing action of Hsc70/DNAJB1/Apg2 progressively introducing nicks in fibrils and

protofilaments of the fibrils, rendering the fibril structure susceptible to breakage during staining on the grid.

Examining sections through reconstructed volumes of fibrils from sucrose gradient fractions 25 (Figure 4) or 16 by electron tomography reveals further details of fibril structure and chaperone-induced fibril disintegration (Figure 4B). Untreated fibrils appear smooth, revealing their substructure composed of four protofilaments (Vilar et al., 2008) (Figure 4A). After incubation with Hsc70/DNAJB1/Apg2 and ATP, however, globular complexes of variable sizes are seen bound to fibril surfaces (Figure 4C and movie S1), as described after negative stain EM (Figure 3D). At sites of fibril breakage we frequently observe fragments consisting of protofibrils or nicked chunks of protofibrils aligned on the grids (Figure 4D and movie S1). These protofibrils are thinner (8-12 nm in diameter) than chaperone-decorated mature twisted fibrils (15-25 nm in diameter, dependent on the twist). Protofibrils appear to be unstable and prone to bind to each other.

Overall our EM analyses suggest that the Hsc70/DNAJB1/Apg2 chaperone combination introduces internal nicks into protofilaments, thereby weakening the fibril structure and generating short protofibril fragments that can dissociate from the fibrils.

Chaperone association to α-Syn fibrils

To obtain molecular insight into the mode of action of Hsc70/DNAJB1/Apg2 we investigated which chaperone components bind to α-Syn fibrils. Upon sucrose gradient centrifugation in the absence of fibrils, chaperones float to the top of the sucrose gradient, reflecting monomeric or indistiguishable very small oligomeric forms (Figure S3C). After incubation of the chaperones with α-Syn fibrils however, individually or in combination, Hsc70 and DNAJB1 are also detected by immunoblotting in fractions 10-19 and 25, as are fibrils. This implies binding of these proteins to fibrils (Figure 3A). The NEF Apg2, when added alone to the fibrils, was detected by immunoblotting only in fraction 25 (Figure 3A, lower panel). When added with DNAJB1 and Hsc70, Apg2 was also present in the shortened fibril fractions 10-19, but at markedly lower levels than the other two chaperones, and was detectable by mass spectrometry (Figure S3D). Binding of all three

chaperones (Hsc70, DNAJB1, Apg2) to shortened α-Syn fibrils treated with the complete chaperone combination was further corroborated by immunogold labeling (Figure 3E).

To determine the structural contributions of the individual components to the active multicomponent machinery, we reconstructed EM-tomograms of fibrils separately treated with Hsc70, DNAJB1 or Apg2, or with the Hsc70/DNAJB1 combination (Figure 4E). Analysis of the reconstructed volumes reveals that each chaperone contributes a distinctive structural signature to the complexes. Hsc70 on its own results in an irregular coating of fine and coarse features (2-5 nm in diameter). DNAJB1 alone coats the fibrils with a uniform layer of about 2-3 nm features with a spacing of about 5 nm along the fibril surface. A sparser decoration is seen for Apg2, with complexes ranging between 5-10 nm in diameter. Hsc70 and DNAJB1 added together result in a combination of their individual features and the fibril surface has a more rough appearance not seen in the individual treatments, which may be due to formation of Hsc70-DnaJB1 complexes or alterations in the fibril structure. These observations confirm that all three chaperones are capable of independently binding to α-Syn fibrils, but also suggest that DNAJB1 binds most efficiently, fully and uniformly coating the surface, consistent with its established role in substrate recruitment.

Kinetics of chaperone interaction with α-Syn fibrils

For dissection of the fibril disassembly mechanism, we quantified the interaction of chaperones and α-Syn fibrils using fluorescence techniques (Figure 5). The binding constants of DNAJB1-fibril and Hsc70-fibril interactions were analyzed by fluorescence anisotropy, which measures changes in rotational diffusion of the fluorescent molecules upon interaction, using Alexa488-labeled DNAJB1-G194C (Alexa488-DNAJB1) and Hsc70-T111C,C267A,C574A,C603A (Alexa488-Hsc70) (Figure 5A). Upon interaction with fibrils, the fluorescence anisotropy of the labeled chaperones changes, allowing to detect and quantify complex formation. Titration of labeled DNAJB1 or Hsc70 (with ATP) with α-Syn fibrils yielded equilibrium dissociation constants (K_D) of 5.6 ± 0.8 μM and 3.1 ± 0.4 μM, respectively.

The affinity of Alexa488-Hsc70 for fibrils increased in the presence of DNAJB1, yielding a K_D of 0.17 ± 0.02 μM. DNAJB1 therefore increases Hsc70's affinity for fibrils strongly, by 18-fold.

We then investigated the kinetics of these interactions. Alexa488-DNAJB1 associated to α-Syn fibrils at a rate too high to be determined accurately in our experimental setup (Figure S4A). The dissociation of Alexa488-DNAJB1 from fibrils was measured by addition of an excess of unlabeled DNAJB1 to the Alexa488-DNAJB1-α-Syn fibrils, which prevents Alexa488-DNAJB1 rebinding to fibrils after it had dissociated. Addition of unlabeled DNAJB1 results in a decrease of anisotropy (Figure S4B), corresponding to a dissociation rate (k_{off}) of 0.0185±0.001 s^{-1}. Based on the measured equilibrium K_D and k_{off}, the calculated rate for Alexa488-DNAJB1 association (k_{on}) to fibrils is 3303 $M^{-1}s^{-1}$. The association kinetics for Alexa488-Hsc70 were determined at various concentrations of α-Syn fibrils (based on the monomer concentration) and all data globally fitted using a second order rate equation (Figures S4D and S4E; Table S1) (Rutkowska et al., 2008). The association of Alexa488-Hsc70 to fibrils in the presence of ATP (123±38 $M^{-1}s^{-1}$; Figure S4D) is about 30-fold slower than the calculated k_{on} for Alexa488-DNAJB1 but is 20-fold accelerated with DNAJB1 present (2539±57 $M^{-1}s^{-1}$; Figure S4E and Table S1). Disrupting the J-protein HPD motif, which is essential for interaction with Hsp70 (Tsai and Douglas, 1996), by mutation to QPN abrogates acceleration of the k_{on} (Figure S4C). We infer DNAJB1 stimulation of the Hsc70 ATPase activity is required for efficient Hsc70 association to α-Syn fibrils.

The presence of DNAJB1 increases the k_{on} of Alexa488-Hsc70 to fibrils by 20-fold, but increases the k_{off} by only 2.6-fold. The K_D of the Alexa488-Hsc70-fibril complex in the presence of DNAJB1 determined directly by equilibrium titration (0.17 μM) is however, 10-fold lower than the K_D calculated from k_{on} and k_{off} values (1.7 μM). This discrepancy may be explained by the existence of biphasic association and dissociation kinetics, similar to those shown for the substrate binding kinetics of other Hsp70s (Pierpaoli et al., 1998), which we cannot resolve in our measurements and precludes precise calculation of K_D values based on k_{on} and k_{off} values. Despite this limitation,

our results unequivocally show that DNAJB1 acts by accelerating the association of Hsc70 with fibrils in the presence of ATP.

We then investigated any effects of NEFs on the release of DNAJB1 and Hsc70 from fibrils. To measure DNAJB1 release we used Alexa594-DNAJB1 (acceptor) and preformed Alexa-488-α-Syn fibrils (donor) in Förster resonance energy transfer (FRET) assays. This allows specific monitoring of interactions between DNAJB1 and α-Syn fibrils in the presence of Hsc70, and avoids background fluorescence anisotropy signals generated from the interaction between Hsc70 and DNAJB1. Addition of Alexa594-DNAJB1 to a population of homogeneous Alexa-488-α-Syn fibrils increased acceptor fluorescence, indicative of interaction (Figures 5B and 5C). In contrast, mixing Alexa594-DNAJB1 and Alexa-488-labeled monomeric α-Syn did not (Figure S4F). DNAJB1 therefore interacts with fibrils but not with monomeric α-Syn-S9C. Addition of Hsc70 without ATP leaves acceptor fluorescence unchanged (Figure 5B and C). However, including ATP drops acceptor fluorescence to levels between those of free and fibril bound Alexa594-DNAJB1. This suggests ATP binding/hydrolysis by Hsc70, or the subsequent Hsc70 binding to α-Syn fibrils, increases the distance between Alexa594-DNAJB1 and α-Syn fibrils. Interestingly, further addition of the NEF Apg2 (Figures 5B and S4G) reduces acceptor fluorescence to similar levels as unbound DNAJB1, though only when Hsc70 is present. We conclude that the interaction of Apg2 with Hsc70 dissociates DNAJB1 from α-Syn fibrils.

To measure Hsc70 release, we monitored effects of Apg2 on the k_{off} of Alexa488-Hsc70 from α-Syn fibrils, using anisotropy measurements. Addition of Apg2 to Alexa488-Hsc70-fibril complexes formed in the presence of DNAJB1 led to a very rapid decrease in anisotropy, which precluded determination of the rate of dissociation (Figures 5D and S4H). This decrease in anisotropy reflects rapid dissociation of Alexa488-Hsc70 from the fibrils. At low Apg2 concentrations anisotropy subsequently slowly increased again, suggesting that after initial dissociation from the fibrils, Alexa488-Hsc70 can slowly rebind and start a new chaperone binding cycle. Our data are consistent with a scenario in which the nucleotide exchange activity of Apg2 accelerates ADP dissociation from Hsc70 followed by subsequent rapid

association of ATP with Hsc70, opening the Hsc70 substrate-binding pocket and triggering substrate release.

Substituting Apg2 with the Hsp70-specific NEF Bag1, which belongs to a distinct protein family, results in dramatically lower rates of Alexa488-Hsc70 dissociation from fibrils (Figure 5D). This holds even at Bag1 concentrations that lead to similar nucleotide exchange rates in Hsc70 as those achieved by Apg2 (Figure S4I). This difference in efficiency of Hsc70 release from fibrils correlates with strongly differing activities of Apg2 and Bag1 in Hsc70-DNAJB1-mediated fibril disassembly. Apg2 accelerates efficient fibril disassembly while Bag1 is poorly effective at all concentrations tested (Figure 5E). Importantly, Apg2 works optimally at substoichiometric Apg2 to Hsc70 ratios of 1:20 to 1:10, and is even inhibitory at higher ratios such as 0.5:1 and 1:1 (Figure S4J and S4K). We conclude that there is high specificity for NEFs of the Hsp110 family as cochaperones for Hsc70-mediated amyloid fibril disassembly.

Fibril-protruding α-Syn regions are essential for disassembly

Biophysical data implicate residues 30 to 110 of each α-Syn molecule in β-structure formation with neighboring α-Syn molecules to form the fibril core structure (Vilar et al., 2008). This leaves the N- and C-terminal regions of each α-Syn molecule relatively flexible and exposed in the fibril (Vilar et al., 2008). We therefore investigated the role of these exposed regions of α-Syn in chaperone action during fibril disassembly.

As previously reported (Vilar et al., 2008), we find that α-Syn$^{30-110}$ fragments form fibrils (Figure 6A). Unlike wt fibrils however, truncated α-Syn$^{30-110}$ fibrils are not disassembled by the Hsc70/DNAJB1/Apg2 machinery (Figure 6B). To pinpoint the critical step preventing disassembly, we investigated the ability of the chaperones to associate with α-Syn or α-Syn$^{30-110}$ fibrils by anisotropy (Figure 6C). Hsc70 associates with α-Syn$^{30-110}$ fibrils, when add separately, but recruitment of Hsc70 to fibrils by DNAJB1 and release of Hsc70 from fibrils by Apg2 is affected in α-Syn$^{30-110}$ fibrils, compared to wt fibrils. It is therefore possible that N- and/or C-terminal parts of the α-Syn molecule provide a specific binding platform for the composite Hsc70/DNAJB1/Apg2 machinery required for formation of the functional

chaperone complex. This result indicates that the N- and C-terminal regions of α-Syn are critical for productive chaperone targeting.

Chaperone-disassembled α-Syn species are less toxic than fibrils

For many amyloidogenic proteins including α-Syn, small, soluble prefibrillar oligomers are more toxic to cells than mature fibrils (Caughey and Lansbury, 2003; Dedmon et al., 2005; Haass and Selkoe, 2007). The ensemble of α-Syn oligomers interact with lipids, disrupt membranes, and kill cells in culture and *in vivo* (Caughey and Lansbury, 2003; Conway et al., 1998, 2000; Danzer et al., 2007; Karpinar et al., 2009; Tsigelny et al., 2008; Winner et al., 2011). Cell toxicity has also been reported for α-Syn fibrils preformed *in vitro* and applied externally to cultured cells (Bieschke et al., 2010; Pieri et al., 2012). A pertinent question therefore is whether fibril disassembly by the human Hsp70 system is beneficial or toxic for cells.

We incubated SH-SY5Y neuroblastoma cells with either preformed α-Syn fibrils or total or soluble fractions of chaperone-treated α-Syn fibrils. Using the MTT cellular viability assay we find that fibrils formed *in vitro* are toxic, whereas α-Syn monomers are not (Figure 7A). Prior incubation of fibrils with Hsc70/DNAJB1/Apg2 and ATP for 4 h slightly reduced toxicity of the total incubation mixture for neuroblastoma cells. Since these reactions contain a mixture of about 80% fibrils and 20% solubilized material we separated fibrils from disassembled soluble material by centrifugation and determined the toxic potential of only the disassembled material, present in the supernatant (Figure 7A). The post-reaction soluble material was significantly less toxic when added externally to cells than the equivalent amount of α-Syn from a total disassembly reaction mixture. We conclude that monomers or very small soluble oligomers of α-Syn, generated from chaperone-mediated fibril disassembly, are less toxic than untreated fibrils.

To further characterize the toxicity of intermediate α-Syn disassembly species we used a two-step purification procedure. We created Avi-tag capped α-Syn fibrils and treated them with the chaperone combination as described (Figure 2B). We separated longer/intact fibrils from disassembled material using streptavidin-coated magnetic beads and further fractionated

disassembled material by centrifugation (Figure 7B). This approach avoids the potential pelleting of newly generated oligomers and fragmented fibrils together with the original fibrils and allows further separation of fragmented fibrils from soluble small oligomers and monomers. In reactions without chaperones, no α-Syn species were liberated from the bead-tethered fibrils and no toxicity was observed for the total (T) and supernatant (S) of the material released from magnetic beads. After 4 h reaction with Hsc70/DNAJB1/Apg2 and ATP total α-Syn material released (T) was still toxic to neuroblastoma cells. Equal concentrations of the soluble supernatant (S) however, is much less toxic to cells than pellet material containing fibril fragments (P). We infer short fibrils and fragments generated by Hsc70 and cochaperones are not less toxic to cells. However, we find that complete depolymerisation of α-Syn fibrils by this chaperone system alleviates toxicity.

Discussion

This study demonstrates that the human Hsc70 chaperone together with DNAJB1 and Apg2 co-chaperones constitutes an unexpectedly powerful ATP-dependent amyloid disaggregase which *in vitro,* solubilizes α-Syn fibrils within minutes. The final products of the disassembly reaction are soluble, largely monomeric α-Syn species which are significantly less toxic when added exogenously to neuroblastoma cells than intact, or fragmented α-Syn amyloid fibrils. Disaggregation directly reverses the accumulation of toxic α-Syn species and amyloid fibrils, and therefore may contribute to the characteristic late onset of Parkinson´s disease, and potentially even revert some pathophysiology. In many organisms furthermore, the capacity of the cellular protein quality control machinery declines during aging (Labbadia and Morimoto, 2015), potentially compromising the disaggregase activity in aged organisms. However, our results also show that incomplete disassembly of α-Syn fibrils by Hsc70/DNAJB1/Apg2 generates short fibrils and oligomeric α-Syn species which are toxic and perhaps even increase amyloid seeding capacity *in vivo*. The pathophysiological manifestation of these Janus head

features of Hsp70-based disaggregase activity probably depends on the balance of cellular proteostasis.

The existence of a powerful amyloid disassembly activity by a human chaperone system demonstrated here contrast earlier reports showing either no activity (Bieschke et al., 2009; Evans et al., 2006; Murray et al., 2013; Murray et al., 2010) or ony weak, up to 720-fold lower activity, requiring 30 days incubation time with chaperones to reach 50% disassembly (Duennwald et al., 2012). The failure to detect a robust Hsp70-based disassembly activity in earlier studies probably reflects the specificity of the Hsp70 machine assembled. Efficient α-Syn fibril disassembly activity requires substoichiometric levels of the NEF relative to Hsc70 and a highly specific set of chaperone components. Regarding the Hsp70s, we find the heat-inducible Hsp70 homolog (HSPA1A) in combination with DNAJB1 and Apg2 disassembles fibrils less efficiently than the constitutive homolog Hsc70 (HSPA8) (Figure S1). Fibril disassembly is evidently therefore a basic "housekeeping" activity of the Hsp70 machinery rather than strictly dependent on the induction of a cellular heat stress response. Regarding the J-proteins, out of those family members tested, only the class B J-protein DNAJB1 disassembles fibrils, while class A J-proteins DNAJA1 (Hdj2) (Figure S1) and DNAJA2 (not shown) did not. Consistent with this scenario, prion propagation in yeast requires the class B J-protein Sis1, but not class A J-protein Ydj1 (Higurashi et al., 2008). Selectivity may be due to finely tuned substrate-specific differences among J-proteins in cooperation with Hsp70. For example, both DNAJA1 and DNAJB1 bind to fibrils (Pemberton et al., 2011) but DNAJB1 is much better than DNAJA1 at promoting the loading of Hsc70 to α-Syn fibrils (data not shown). Regarding the NEFs, members of the Hsp110 class (Apg2 and Hsp105) strongly enhance the protein disaggregation activity of Hsc70/DNAJB1, but Bag-type NEF Bag1 (which lacks ATPase activity) does not (Figures S1 and 5E). The basis for these differences is unclear.

Disassembly of α-Syn fibrils by Hsc70/DNAJB1/Apg2 occurs through ATP-dependent fragmentation (severance) and depolymerization. This dual mechanism generates smaller fibrils, oligomers and monomeric α-Syn, which we detected by (i) gel filtration of supernatant fractions of chaperone-treated fibrils, (ii) native gel electrophoresis of species released from biotinylated

fibrils, (iii) size fractionation via gradient centrifugation and (iv) EM. The main argument supporting a dual fragmentation-depolymerisation mechanism is the time course reflecting when these species are generated during the reaction. Fragmentation of large fibrils into significantly shorter ones occurs within a few minutes, well before corresponding amounts of solubilized (e.g. monomeric) α-Syn species appear. Depolymerisation to monomers, on the other hand, occurs at time points (e.g. during early and late phases of the reaction) when fragmentation processes alone cannot account for these products. Liberation of single α-Syn molecules from fibril ends is most likely energetically less demanding than extraction of molecules from internal sites. We therefore assume depolymerisation occurs predominantly at preexisting fibril ends and at protofilament and fibril ends newly generated by fragmentation.

The relative contribution of depolymerisation versus fragmentation to the overall disassembly reaction is difficult to assess. Based on the kinetics of monomers and fragmented (i.e. completely physically detached) fibril appearance during chaperone action, we estimate generation of solubilized α-Syn monomers via depolymerisation is approximately 1000-fold faster than fibril fragmentation (see results for detailed calculation). However, this estimate does not take into account the generation of “nicked” fibrils, during which individual protofilaments are severed by the action of chaperones, but remain attached to fibrils through the hydrophobic and electrostatic interactions between the four intertwined protofilaments of the mature α-Syn fibrils (Khurana et al., 2003). The existence of such nicked fibrils is indicated by EM images of fibril disintegration sites, and likely accounts for “fragile fibrils” generating aligned arrays of short fibrils in many EM images (Figures 3D, 4D, S2A and S3E). Tomogram analysis of fragmentation sites shows parallel protofibrils, chunks of protofibrils and globular oligomers attached to each other and to unnicked protofibrils. We speculate that through nicking of individual protofilaments/protofibrils, the chaperones weaken fibrils against tensile and shearing forces generated during negative stain EM preparation. Ultimately this nicking activity will generate protofilament and protofibril fragments that are short enough to dissociate from the fibrils and lead to complete fibril fragmentation. Nicking activity will substantially increase the number of new filament ends, facilitating chaperone-mediated, or even

spontaneous depolymerisation. This suggests depolymerisation becomes increasingly important during ongoing fibril disintegration since more free labile protofilaments and fibril ends are generated. This may explain why shortened fibrils (fractions 10-19 in sucrose density gradients; Figures 3A and S3B) are not detectably further fragmented, but instead are converted rapidly to α-Syn monomers. This disassembly reaction feature may allow limiting formation of shorter, more toxic α-Syn fragments and oligomers with amyloid seeding capacity.

What is the molecular basis for the disassembly reaction? Using immunogold labeling, negative stain EM and electron-tomography we detect all three Hsc70, DNAJB1 and Apg2 components on fibril surfaces and provide 3D-snapshots of the ongoing chaperone actions on fibrils. This is the first direct demonstration of association of Hsp110 with a substrate *in vitro* and also, the first visualization of a human disaggregase system bound to an amyloid substrate. Although each chaperone can separately associate with fibrils, disassembly requires the concerted action of all three components. Consistent with this, the range of differently sized globular structures that decorate fibrils in the presence of Hsc70/DNAJB1/Apg2 and ATP, includes larger structures, which most likely are dissociated α-Syn oligomers, not present when chaperones were added separately (Figures 3, 4 and S3E).

Kinetic analysis of the concerted action of Hsc70/DNAJB1/Apg2 on α-Syn fibrils leads to the model of fibril disassembly shown in Figure 7C. DNAJB1 rapidly associates with fibrils and accelerates subsequent recruitment and binding of Hsc70 by stimulating the ATPase activity of Hsc70. Binding of Apg2 then leads to rapid dissociation of Hsc70, DNAJB1 and Apg2 itself. The Apg2-stimulated dissociation step of all three chaperones is critical for fibril disassembly. Specifically, the DNAJB1-mediated association of Hsc70 with fibrils followed by chaperone dissociation through spontaneous nucleotide exchange (in the absence of Apg2) is inefficient in triggering fibril breakage or depolymerization. We surmise the allosterically controlled, coordinated dissociation of all three chaperone components from the fibrils involves physical forces that generate the power stroke required for extraction of α-Syn molecules.

Several features of this functional chaperone cycle are consistent with the current model of the Hsp70 cycle (Mayer, 2013). Our results however, also reveal novel aspects, particularly relating to the role of the NEF. First, Apg2 promotes dissociation from the substrate of both Hsp70 and DNAJB1. This contradicts a previous “clamping and walking mechanism” proposed for Hsp110, Hsp70 and J-proteins acting on a substrate (Mattoo et al., 2013). That mechanism predicts that Hsp110 increases the lifetime of all three components on the surface of the aggregate during cooperative action, the opposite of what we find here. Second, Apg2 greatly accelerates the dissociation of Hsc70 and DNAJB1 from fibrils even at reactant concentrations which, in the absence of fibrils, only partially stimulate nucleotide exchange by Hsc70 (Figure S4I). Perhaps the local environment of the Hsc70/DNAJB1/Apg2 complex on the fibril surface, together with Apg2 binding to the fibril, specifically targets Apg2 to Hsc70 for nucleotide exchange. Third, in contrast to Apg2, Bag1 hardly stimulates Hsc70 dissociation from fibrils and fibril solubilization, even at concentrations where Bag1 and Apg2 NEF activities are comparable. This suggests either a NEF-independent role of Apg2 in fibril disassembly or a finely tuned regulation of the NEF activity of Apg2 in concert with Hsc70, DNAJB1 and fibrils, to which Bag1 is insensitive.

A salient finding is that deletion of the N- and C-terminal regions of α-Syn (α-Syn$^{30-110}$) protruding from the fibril axis (Vilar et al., 2008) completely abrogates fibril disassembly by Hsc70/DNAJB1/Apg2. Unexpectedly, chaperone association per se is not compromised. Instead the cooperation, at least between Hsc70 and DNAJB1, leading to the correct targeting and activation of Hsc70, is defective. We surmise the truncated α-Syn$^{30-110}$ fibrils lack the local environment permitting the ordered association of the three chaperone components needed to generate the powerstroke driving disassembly. α-Syn$^{30-110}$ fibrils may in addition have subtle structural differences to wt-α-Syn fibrils which confer increased resistance to disassembly activities.

In conclusion our findings demonstrate efficient reversal of α-Syn fibril formation by a specific human Hsp70 chaperone network. This adds a new layer of complexity to the biology of amyloid protein fibrils. Definition of

parameters influencing the cellular α-Syn fibril disaggregase activity, including cooperation with other components of the chaperone network, should contribute to defining the pathophysiology of Parkinson´s disease and clarify apparent links to the mechanisms of aging. Understanding the biology and molecular mechanism of fibril disaggregation should also facilitate effective therapeutic interventions. Finally, determining the spectrum of amyloid proteins subject to Hsp70 network-dependent disaggregation should inform on the extent to which this disaggregase activity may be relevant for other amyloid protein-driven diseases.

Acknowledgements

We thank Kang Chi for purified Apg2,Ingrid Hausser, Jacomine Krijnse-Locker and Androniki Kolovou for help with EM experiments and Daniel Kofi Clare for direct electron detector and tomography setup. Stain OW40 was provided by the CGC, which is funded by NIH Office of Research Infrastructure Programs (P40 OD010440). This work was supported by grants of the Deutsche Forschungsgemeinschaft (to BB and MPM), Wellcome Trust grants (to HRS) and fellowships of the Alexander von Humboldt Foundation (to NBN and ASz).

Contributions

XG and BB conceived the study. XG, MC, CN, AM, HS, MPM and BB designed the experiments. XG, MC, CN and AS performed the experiments. XG, MC, CN, HS, DLG, NBN, MPM and BB analyzed the data. XG, MPM, NB, DLG and BB wrote the manuscript.

Competing interests

The authors declare there are no competing interests.

Experimental procedures

Fluorescent dyes and antibodies

Alexa Fluor dyes were purchased from Life Technologies GmbH (Darmstadt, Germany). Mouse monoclonal antibodies against α-Syn (full length or truncation), Hsc70, GFP and rabbit polyclonal antibodies against DNAJB1 were purchased from Santa Cruz Biotechnology (Texas, USA), Acris Antibodies GmbH (Herford, Germany), Covance Inc. (Princeton, NJ, USA) and Enzo Life Sciences GmbH (Lörrach, Germany), respectively. Rabbit polyclonal antibodies against Hsc70 and Apg2 were produced by Charles River Laboratories (Sulzfeld, Germany).

Protein expression and purification

Human Hsc70, Apg2, Hsp105α, DNAJB1, Hdj2, Avi-tagged α-Syn were expressed in *E. coli* BL21 (DE3) with an N-terminal His6-Smt3-tag and purified by affinity chromatography and gel filtration as published earlier (Andreasson et al., 2008; Rampelt et al., 2012). After affinity purification the His-Sumo tag was cleaved off with SUMO-protease Ulp1. All the cleaved products were applied to fresh protino beads to remove His-Sumo and Ulp1. The flow though was collected and used for further purification. After cleavage and removal of the tag and Ulp1, DNAJB1 was further purified by cation exchange chromatography using a SP sepharose column, Hsc70 and Hdj2 were further purified by Superdex 75 gel filtration in a buffer containing 50 mM Hepes pH 7.5, 150 mM KCl and 5% glycerol, and the remaining proteins were concentrated and frozen at -80°C. The gene encoding α-Syn was cloned into pTYB11 (intein/chitin-binding domain system; New England Biolabs) and purified following manufacture's recommendations (Uversky et al., 2001), followed by further purification by gel filtration in a buffer containing 50 mM sodium phosphate, pH 7.5 and 100 mM NaCl. The α-Syn, Hsc70 and DNAJB1 point mutants were generated by PCR mutagenesis and standard cloning techniques and were verified by sequencing. His-Sumo-α-Syn fragment was obtained by fusion PCR and cloned into pTrc plasmid using NdeI and BamHI sites to generate a gene encoding His-Sumo-α-Syn-Avi-tag. pTrc-His-Sumo-α-Syn-Avi was co-overexpressed with the gene encoding

biotin-[acetyl-CoA-carboxylase] ligase BirA in *E. coli* to generate C-terminal biotin labeled α-Syn. Biotin was added to the culture medium at a final concentration of 40 mg/l. The C-terminal biotin labeled α-Syn was purified by affinity purification as described above. The purity of proteins was verified by SDS-PAGE and was generally >90%.

Fibril formation

To produce mature, long fibrils, 200 μM gel filtration purified α-Syn or α-Syn-S9C monomers were filtered through 0.2 μm filters and incubated in 1.5 ml-microfuge tubes at 37℃ under orbital shaking (1000 rpm) at 37°C for 1 week in a buffer containing 50 mM sodium phosphate pH 7.3, 100 mM NaCl and 0.05% sodium azide. EM imaging confirmed that our preparations contained mature fibrils and no amorphous aggregates or small beta-sheet aggregates.

Fluorescent labeling of proteins and fibrils

Purified Hsc70-T111C,C267A,C574A,C603A (100 μM), DNAJB1-G194C (150 μM) or α-Syn-S9C monomer (85 μM) were incubated with a tenfold excess of Alexa Fluor® 488 C5 maleimide (Alexa488) or Alexa Fluor® 594 C5 maleimide (Alexa594) at room temperature for 2 h (in excess of ATP for Hsc70 to avoid labeling the only remaining essential Cys17) followed by chromatography through a PD-10 desalting column (GE healthcare) to remove free dye. Labeling efficiency was monitored by nanodrop, using absorption at A_{280} (DNAJB1ε_{280} = 19035 $M^{-1}cm^{-1}$, Hsc70ε_{280} =33600 $M^{-1}cm^{-1}$, α-Synε_{280} = 5069 $M^{-1}cm^{-1}$) for protein concentration and absorption at A_{493} for Alexa488 (ε_{494} = 72000 $M^{-1}cm^{-1}$), A_{588} for Alexa594 (ε_{590} = 96000 $M^{-1}cm^{-1}$). The labeling efficiency was 100% as determined by protein and dye concentrations. The activity of labeled chaperones was comparable to that of the wild type proteins as measured by a luciferase disaggregation assay (Rampelt et al., 2012). For the labeling of α-Syn-S9C fibrils, 200 μM preformed α-Syn-S9C fibrils were incubated with a tenfold excess of Alexa488 at room temperature for 2 h followed by centrifugation at 16,000 g for 15 min at 4℃ to remove free dye. Then the fibril pellet was washed three times with

50 mM Hepes-KOH pH 7.5, 150 mM KCl, 5 mM $MgCl_2$ buffer to remove dye non covalently bound to fibrils. Fibrils were dissolved in 8 M guanidine chloride (GdnHCl) and the labeling efficiency was measured by nanodrop, using absorption at A_{280} (α-Synε_{280} = 5960 $M^{-1}cm^{-1}$) for protein concentration and absorption at A_{493} for Alexa488 (ε_{494} = 72000 $M^{-1}cm^{-1}$) concentration. The fibril labeling efficiency was normally around 70-90% as determined by protein and dye concentrations.

Sedimentation assay (supernatant-pellet centrifugation)

α-Syn fibrils were incubated in disaggregation buffer (50 mM Hepes-KOH pH 7.5, 50 mM KCl, 5 mM $MgCl_2$, 2 mM DTT supplemented with 2 mM ATP and ATP regeneration system (3 mM PEP, 20 ng/µL pyruvate kinase (PK)) and incubated with the indicated chaperones for different time intervals at 30°C. ATP, PEP and pyruvate kinase were omitted when necessary (-ATP). The fibril-chaperone mixture was centrifuged at 16,000 g for 30 min at 4°C. α-Syn levels in the supernatant or pellet were measured by western blot using α-Syn mouse monoclonal antibodies. Quantification of blots was done using ImageJ software.

Fluorescence de-quenching assay and size exclusion chromatography

Alexa488 labeled α-Syn-S9C monomers or preformed α-Syn-S9C fibrils (0.5 µM protomer) were incubated with 8 M guanidine chloride (GdnHCl) or different combinations of chaperones in the disaggregation buffer at 30°C. Disaggregation of labeled fibrils was determined by monitoring Alexa488 fluorescence intensity at 515 nm (excitation wavelength 488 nm) on a Perkin-Elmer LS 50B fluorescence spectrometer. Gel filtration of supernatant fractions from disassembled, fluorescently labeled α-Syn-S9C fibrils was performed using an analytical Superdex 75 10/300 GL column (GE Healthcare) at 25°C in 50 mM Hepes pH 7.5, 150 mM KCl, 5% glycerol. Eluted fractions were collected automatically and the fluorescence intensity of each fraction was measured by a Jasco fluorophotometer FP-6500.

Negative stain EM

10 µl samples were applied to Formvar- and carbon-coated 100-mesh copper grids (Electron Microscopy Sciences) and incubated for 5 min. Grids were rinsed two or three times (for sucrose gradient samples) with 15 µl of de-ionized water and negatively stained with 2% (w/v) uranyl acetate. Excess stain was removed by blotting and air drying. Samples were visualized with an 80 kV Zeiss EM-900. Fibril length was measured manually using ImageJ software.

Fibril fragmentation assay

Biotin-labeled α-Syn-Avi monomers were mixed with wild type fibrils (200 µM monomer concentration, preformed for 7 days) at a ratio of 1:100 and incubated for 4 days at 37°C. Heterofibrils (Avi-tag capped fibrils) were used to monitor fibril fragmentation according to the method of Inoue and Yoshida (Inoue and Yoshida, 2006). Briefly, heterofibrils were incubated with streptavidin-coated paramagnetic beads (Dynabeads® MyOne™ Streptavidin T1, Invitrogen/Life Technologies) at a ratio of fibrils volume:beads slurry of 1:1. To remove excess and non-biotinylated fibrils the beads were washed at least 9 times with 50 mM Hepes-KOH pH 7.5, 50 mM KCl, 5 mM $MgCl_2$, 2 mM DTT buffer containing 1% Triton X-100, followed by a single wash with disaggregation buffer. 5 µl aliquots of the bead-bound fibrils were incubated with chaperones in disaggregation buffer at 30°C for different time intervals. Disassembled wild type fibrils and soluble species were separated from bead-tethered fibrils by immobilizing the paramagnetic beads in a magnetic field.

Native polyacrylamide gel electrophoresis (Native PAGE)

Protein samples were diluted into loading buffer without SDS or any reducing agents and then applied to a 10% Bis-Tris native gel. Gel electrophoresis was performed at 120 V for 2 h in 50 mM MOPS, 50 mM Tris, 1 mM EDTA followed by western blot analysis.

Sucrose gradient centrifugation

α-Syn fibrils (10 µM monomer concentration) or monomers (10 µM) were incubated with or without individual or combinations of chaperones (10 µM Hsc70, 5 µM DNAJB1, 1 µM Apg2) in the disaggregation buffer at

30°C for the indicated time intervals. Then 350 µl of the reaction mixture was applied to 12 ml of a 15-60% sucrose gradient and centrifuged at 86,419 g (35,000 rpm) for 2.5 h at 4°C. After centrifugation, 500 µl fractions were manually removed with a 1 ml-pipette. 25 fractions were taken in total for each sample. The volume of the last fraction was adjusted to 500 µl. Each fraction was mixed by inverting 8-10 times and aliquots (100 µl) were taken for SDS PAGE and immunoblotting. Glycerol was omitted from the SDS-sample buffer. Relative amounts of α-Syn in each fraction after immunoblotting were quantified using imageJ for each time point.

Fibril length measurement and α-Syn protomer calculation

Fibrils incubated with or without chaperones for different time points were subjected to negative EM. EM pictures were randomly chosen and the lengths of 600 fibrils were measured using ImageJ software manually. Untreated fibrils have an average length of 1000 nm. Fibrils with lengths below 500 nm at each time point were grouped as short fibrils and the averaged length of short fibrils was calculated (254 nm). The structural model of α-Syn fibrils suggests one mature fibril consists of 4 protofilaments and the distance between two packed α-Syn protomers is 4.7 Å (Vilar et al., 2008). Based on the average length of the short fibrils and the protomer arrangement in the structural model of α-Syn fibrils, we estimate that 1 short fibril consists of, on average, 2000 α-Syn protomers.

Immunogold labeling

10 µl of sucrose gradient samples were incubated with grids for 5 min followed by blocking. Then the grids were incubated with rabbit anti DNAJB1, Hsc70 or Apg2 antibodies at 1:30, 1:2 and 1:1, respectively. Secondary immunogold-labelling was with goat anti-mouse or goat anti-rabbit IgG conjugated with 5-nm, 15-nm and 5-nm gold (Jackson ImmunoResearch Laboratories).

Electron tomography

Tilt series of negative stain samples of fibrils and chaperones were collected with SerialEM (Mastronarde, 2005) at 3° increments over a range of

± 60°, with a defocus of 1 to 2 µm. Images were recorded on a 200 kV Tecnai F20 EM (FEI) using a DE20 direct electron detector (Direct Electron, LP) at a nominal magnification of 13 000× (corresponding to a pixel size of 3 Å). Fiducial-free alignment of tilt images and tomogram reconstructions was carried out in IMOD (Kremer et al., 1996). For each combination of chaperones, 15 to 20 tomograms were reconstructed and analyzed.

C. elegans *strains and maintenance*

Wild-type (N2, Bristol) and transgenic animals were maintained using standard methods (Brenner, 1974). Nematodes were grown on NGM plates seeded with *E. coli* strain OP50 at 20°C. The strain OW40 *zgIs15[unc-54p::alpha-synuclein-WT::yfp]IV* was obtained from the *Caenorhabditis* Gene Center (CGC).

Isolation of detergent-insoluble α-*Syn from* C. elegans

Nematodes expressing alpha-synuclein::YFP were age-synchronized by bleaching; gravid adult animals were treated with hypochloride bleaching solution (5,5 ml H_2O; 2,5 ml 1M NaOH; 2 ml 5% hypochloride) and isolated eggs were hatched overnight in M9 buffer. 1000 synchronized L1 larvae were transferred onto each of 20 OP50 seeded 10 cm NGM plates and grown for 4 days until they reached day two of adulthood. Animals were collected, washed in M9 buffer and suspended in lysis buffer (20 mM Tris, pH 7.5; 10 mM β-mercaptoethanol; 0.5% Triton X-100) supplemented with complete protease inhibitor (Roche) before shock-freezing in liquid nitrogen. Proteins were extracted by adding 0.7 mm diameter Zirconia beads (BioSpec) and vortexing for 6 cycles of 60 s at max. and 20 s rest speed in a Vortex-Genie at 4°C, followed by further cell lysis on ice. The lysate was cleared from carcasses by centrifugation at 5000 rpm for 2 min at 4°C in a tabletop centrifuge. The lysate was mixed with 1% N-Lauroylsarcosine (Sarkosyl NL), followed by ultracentrifugation at 254,000 g for 2 h at 4°C. Pellet fractions were resuspended in 100 µl of 50 mM Hepes (pH 7.5), 50 mM KCl and 5 mM $MgCl_2$ buffer and washed twice to remove residual Sarkosyl NL. The final total protein concentration was around 500 µg/ml.

MTT assay

SH-SY5Y cells were cultured in Dulbecco's modified Eagle's Medium F12 (Gibco) supplemented with 10% (v/v) fetal bovine serum at 37°C in 5% CO_2. Cells were plated at a density of 5×10^3 cells/well in 96-well plates (Costar) and incubated for 24 h at 37°C in 5% CO_2. The medium was then replaced, and the fibril samples and controls (buffer alone or chaperone mixture alone) were incubated with cells for 24 h. Cell viability was measured using a CellTiter 96® Non-Radioactive Cell Proliferation Assay kit (Promega). Briefly, MTT (3-(4,5-Dimethylthiazol-2yl)-2,5-diphenyltetrazolium bromide) was added to cells and incubated for 4 h. The quantity of formazan generated (proportional to the number of viable cells) was measured by absorbance at 570 nm using a plate reading spectrophotometer.

Fluorescence anisotropy

For steady state fluorescence anisotropy experiments purified DNAJB1-G194C and Hsc70-T111C,C267A,C574A,C603A were labeled with Alexa Fluor® 488–C5–maleimide or Alexa Fluor® 594–C5–maleimide. 0.1 μM labeled protein was incubated with increasing concentrations of preformed α-Syn fibrils for 30 min at 25°C and changes in fluorescence anisotropy were determined using fluorophotometer FP-6500 (Jasco). Anisotropy values were converted into percentage of protein bound to fibrils at a given fibril concentration after corrections for changes in quantum yields. The one-site binding model was fitted to the data using GraphPad Prism® 6.0 (GraphPad software; San Diego, CA, USA). Association of labeled chaperones was monitored by the change of anisotropy with time at 25°C. Competition of alexa488-DNAJB1 with unlabeled DNAJB1 was measured by incubation of 0.1 μM Alexa488-DNAJB1 with 3 μM α-Syn fibrils for 30 min at 30°C, followed by the addition of 50 μM unlabeled DNAJB1. Changes in fluorescence anisotropy with time were determined and fitted by a one-phase decay model using GraphPad Prism.

For time-resolved anisotropy, the association kinetics of Hsc70 to α-Syn fibrils was measured for different α-Syn fibril concentrations (based on

the monomer concentration) and all data globally fitted by the second order rate equation (Rutkowska et al., 2008) using GraphPad Prism.

Förster resonance energy transfer (FRET) measurements

For FRET experiments, 0.2 μM Alexa488-labeled preformed α-Syn-S9C fibrils (calculated on the basis of the monomers) or monomers (donor) were mixed with 1 μM Alexa594-labeled DNAJB1 (acceptor) in 25 mM HEPES pH 7.5, 50 mM KCl and 5 mM $MgCl_2$, and allowed to equilibrate for 30 min at 30˚C before measuring the steady-state fluorescence. For competition experiments, 14-fold excess (relative to acceptor concentration) of unlabeled Hsc70, 2 mM ATP and 0.7 μM Apg2 was added sequentially and allowed to equilibrate for 20 min at 30˚C. Emission spectra were recorded on a Jasco FP6500 spectrofluorometer between 500 and 700 nm, at an excitation wavelength of 488 nm for Alexa488 (donor fluorophore). Increase in acceptor emission (at 611 nm for Alexa594) was quantified. For quantification, acceptor fluorescence of Alexa594-labeled DNAJB1 excited at 488 nm was subtracted. The Förster radius of the Alexa488-Alexa594 FRET pair is 60 Å (Spence and Johnson, 2010). All samples were measured at least in duplicate. FRET efficiency was calculated based on the increase of acceptor fluorescence and presented as a percentage of acceptor fluorescence in the absence of competitors.

Figure Legends

Figure 1. ATP-dependent solubilization of α-Syn fibrils by joint action of Hsc70, DNAJB1 and Apg2.

(A) Representative negative stain EM image of α-Syn fibrils assembled for one week at 37°C. (B) Solubilization of α-Syn fibrils detected by sedimentation assay. α-Syn fibrils (2 μM monomer concentration) were incubated in disaggregation buffer with individual or combinations of Hsc70, DNAJB1 and Apg2 (at 2 μM, 1μM, 0.2 μM respectively) in the presence or absence of ATP and ATP regeneration system for 4 h, subjected to centrifugation and solubilized α-Syn detected in the supernatant by immunoblotting. (C) Fibril solubilization kinetics. α-Syn fibrils (2 μM monomer) were incubated with different concentrations of Hsc70 (2 μM, 4 μM and 10 μM as indicated), DNAJB1 and Apg2. The molar ratio of Hsc70:DNAJB1:Apg2 was kept constant at 1:0.5:0.1. The percentage of disassembled soluble α-Syn species in the supernatant versus incubation time is plotted. The inset shows a zoom into the first 60 min. (D) Size exclusion chromatography of solubilized α-Syn fibrils. 4 μM Alexa488-α-Syn-S9C monomers (black, dashed line), soluble fractions of 8M GdnHCl denatured fibrils (red solid line) and fibrils treated for 4 h with chaperones (Hsc70:DNAJB1:Apg2 = 2:1:0.2 μM blue and 10:5:1 μM black solid lines) were subjected to size exclusion chromatography. Fluorescence intensity of Alexa488 was monitored for fractions collected from each sample. The absorbance of 20 μM purified α-Syn-S9C monomers at 280 nm was recorded as control. (E) Relative amounts of monomers and oligomers separated in (D) calculated from the fluorescence intensities. (F) Sedimentation assay. Sarkosyl-insoluble α-Syn-YFP aggregates isolated from *C. elegans* were incubated with disaggregation buffer control or Hsc70/DNAJB1/Apg2 (10 μM/5 μM/1 μM) for 4 h, subjected to centrifugation and solubilized α-Syn detected in the supernatant by immunoblotting using mouse monoclonal anti-GFP antibodies. (G) Sedimentation assay. α-Syn$^{30\text{-}110}$ fibrils (2 μM monomer) were incubated with indicated chaperones (2 μM Hsc70/1 μM DNAJB1/0.2 μM Apg2) for 4 h and then centrifuged at 16,000 g for 30 min at 4°C. Disassembled soluble α-Syn$^{30\text{-}110}$ species in the

supernatant were detected by immunoblotting using α-Syn-60-95 mouse monoclonal antibodies.

Figure 2. Hsc70/DNAJB1/Apg2 chaperones fragment α-Syn fibrils.

(A) Time evolution of the length distribution of chaperone-treated fibrils. 2 μM α-Syn fibrils (monomer concentration) were incubated with 2 μM Hsc70, 1 μM DNAJB1 and 0.2 μM Apg2 for 2 to 1440 min as indicated. EM pictures were taken from negative stain samples for each time point. The lengths of 600 fibrils were measured using ImageJ software and plotted as a histogram of fibril length distribution. (B) Flow diagram of the fibril fragmentation assay. Preformed α-Syn fibrils were incubated with *in-vivo*-biotinylated Avi-tagged α-Syn to form heterofibrils (Avi-tag capped fibrils). Heterofibrils were bound to streptavidin-coated paramagnetic beads, treated with Hsc70/DNAJB1/Apg2 and released material separated from bead-tethered fibrils in a magnetic field (method). (C) Characterization of α-Syn species released from magnetic beads upon chaperone treatment. Bead-tethered α-Syn heterofibrils (roughly 2-10 μM) were incubated with 4 μM Hsc70, 2 μM DNAJB1 and 0.4 μM Apg2 at 30℃ for 2 h or 4 h in the absence or presence of 2 mM ATP. α-Syn levels in the bead-separated supernatant were measured by immunoblotting. (D) EM images of untreated heterofibrils and α-Syn species released from the beads by chaperone treatment. Scale bar, 250 nm.

Figure 3. Combined Hsc70/DNAJB1/Apg2 activity efficiently disassembles α-Syn fibrils into monomers and short fibrils.

(A) Analysis of fibril disassembly reactions by sucrose gradient centrifugation. 10 μM α-Syn monomers, fibrils or fibrils incubated with 10 μM Hsc70, 5 μM DNAJB1, 1 μM Apg2 for 4 h were subjected to sucrose gradient centrifugation. Distributions of α-Syn or chaperone proteins in each fraction (total 25 fractions) were detected by immunoblotting using specific antibodies as indicated to the right. Fractions 1 to 4 (group I), 10 to 19 (group II) and 25 (group III) represent monomers, short fibrils, and unfragmented fibrils, respectively. (B) Representative EM images of α-Syn species of different sucrose gradient fractions (F1, F11, F15, F25) from chaperone-treated fibrils

shown in (A). Scale bar, 1 µm. (C) Time course of a fibril disassembly reaction separated by sucrose gradient centrifugation. Relative amounts of α-Syn in each of the three groups in (A) were quantified by immunoblotting for every time point. (D) Captured fragmentation events. Left panel, untreated α-Syn fibrils from fraction 25 of the sucrose gradient centrifugation. Right panel, α-Syn fibrils in sucrose gradient fraction 15 separated from disassembly reaction containing the full chaperone system. Aligned short separate fibrils decorated with globular structures (right, white arrows). Scale bar, 50 nm. (E) Immunogold labeling of Hsc70 (15 nm gold), DNAJB1 (5 nm gold) and Apg2 (5 nm gold) in sucrose gradient fraction 15 separated disassembly reaction containing the full chaperone system. Scale bar, 100 nm.

Figure 4. Chaperone interaction with α-Syn fibrils and fibril disintegration visualised by electron tomography.

(A) Section through a tomogram of α-Syn fibrils, averaged over 15 z-slices. The area boxed in red is enlarged on the right. (B) Schematic diagram showing section planes through the tomogram, with 1 and 2 indicating upper and central slices, respectively. (C-D) Section through a tomogram of α-Syn fibrils binding the full chaperone complement (C) and fragmented fibrils (D) averaged over 15 z-slices. Right, enlarged views of the boxed region, shown for the upper and central section planes of chaperone decorated fibrils (C) or fragmented fibrils with original mature fibril (yellow line), parallel protofibrils (white lines) and nicked protofibrils (white arrows) (D). (E) Sections through the tomograms of α-Syn fibrils alone, with each chaperone separately, and with Hsc70/DNAJB1. Scale bars, 20 nm.

Figure 5. DNAJB1 accelerates Hsc70 loading onto α-Syn fibrils and Apg2 triggers release of Hsc70 and DNAJB1.

(A) Steady-state fluorescence anisotropy changes upon addition of α-Syn fibrils to Alexa488-DNAJB1 or Alexa488-Hsc70 (0.1 µM). Anisotropy values were converted into percentage of protein bound to fibrils at a given fibril concentration (monomer concentration) after corrections for changes in quantum yield. Binding curves of Alexa488-DNAJB1 (left), Alexa488-Hsc70 in the absence (middle) or presence of 0.05 µM DNAJB1 (right) were fitted by a

one-site binding model using GraphPad Prism. (B) Hsc70, Apg2 and ATP lead to release of DNAJB1 from fibrils. Fluorescence emission spectra of Alexa488-α-Syn-S9C fibrils (green), Alexa594-DNAJB1 (red), and mixtures of both in the absence (black) and presence of Hsc70 (brown), Hsc70+ATP (purple), and Hsc70+ATP+Apg2 (blue). The sum of the individual spectra of Alexa488-α-Syn-S9C-fibrils and Alexa594-DNAJB1-G194C is the dashed orange line. The concentrations for Alexa488-α-Syn-S9C-fibrils, Alexa594-DNAJB1, Hsc70, Apg2 and ATP are 0.2 μM, 1 μM, 14 μM, 0.7 μM and 2 mM, respectively. Fluorescence excitation at 488 nm, emission detected at 611nm with a 20 nm slit. (C) Relative acceptor fluorescence in the presence of different chaperones (minimum 3 measurements) shown in (B). Error bar = standard error of the mean. (D) Apg2 leads to rapid release of Hsc70. Fluorescence anisotropy traces of Alexa488-Hsc70 (0.1 μM) in the presence of DNAJB1 (0.05 μM) and α-Syn fibrils (0.6 μM). In separate reactions Apg2 or Bag1 was added to the reactions at time point 300 s as indicated. (E), Fibril disassembly activity in the presence of Hsc70 (2 μM) and DNAJB1 (1 μM) and absence or presence of different nucleotide exchange factors as indicated.

Figure 6. Inability of Hsc70 chaperone system to disassemble α-Syn$^{30-110}$ fibrils.

(A) Representative negative stain EM image of α-Syn$^{30-110}$ fibrils assembled for one week at 37°C. (B) Sedimentation assay. α-Syn$^{30-110}$ fibrils (2 μM monomer) were incubated with indicated chaperones (2 μM Hsc70/1 μM DNAJB1/0.2 μM Apg2) for 4 h and then centrifuged at 16,000 g for 30 min at 4°C. Disassembled soluble α-Syn$^{30-110}$ species in the supernatant were detected by immunoblotting using α-Syn-60-95 mouse monoclonal antibodies. (C). Anisotropy changes upon binding of Alexa488-Hsc70-T111C (0.1 μM) to α-Syn or α-Syn$^{30-110}$ fibrils (3 μM) in the absence or presence of DNAJB1 (0.05 μM) and dissociation of fibril-bound Alexa488-Hsc70-T111C triggered by Apg2 (0.45 μM). Dissociation of Hsc70 from fibrils was triggered by adding Apg2 at 900 sec as indicated.

Figure 7. Cell toxicity of disassembled α-Syn species and model for chaperone action in fibril disassembly.

(A) α-Syn fibrils or monomers (2 μM protomers) were incubated with or without Hsc70 (2 μM), DNAJB1 (1 μM) and Apg2 (0.1 μM) for 2 h. Total mixture (T, final concentration of α-Syn 0.2 μM) or supernatant after centrifugation at 16,000 g for 30 min (S, final concentration of α-Syn 0.04 μM) was added to culture medium of SH-SY5Y cells for 24 h. Cell toxicity was measured by MTT reduction. (B) α-Syn species released from bead-tethered fibrils (T) in the absence of chaperones (blue bars) or presence of Hsc70/DNAJB1/Apg2 (red bars) and the soluble (S) or pellet (P) fractions of these reactions were added to culture medium of SH-SY5Y cells for 24 h. Cell toxicity was measured by MTT reduction. The final concentration of α-Syn was 0.01 μM (protomer) in the total chaperone-released fraction and 0.0033 μM in the supernatant of this reaction. Final concentration of Hsc70 in the medium was 0.25 μM. (C) Model for chaperone-mediated disassembly of α-Syn fibrils. Individual DNAJB1 (blue), Hsc70 (purple) and Apg2 (green) chaperone components interact with α-Syn fibrils (yellow). In the presence of the complete Hsc70/DNAJB1/Apg2 system, however, DNAJB1 binds rapidly along the entire length of fibrils (step 1) and recruits Hsc70 in the ATP (T) state, which Hsc70 hydrolyzes, converting Hsc70 to the ADP (D) state, forming DNAJB1-Hsc70 complexes on the fibril surface (step 2). The DNAJB1-Hsc70 mediated reaction on its own confers only low basal fibril disassembly activity. Binding of the NEF Apg2 to the DNAJB1-Hsc70 complex catalyzes ADP release from Hsc70 (step 3), followed by rebinding of ATP to Hsc70. This promotes rapid release of Hsc70, DNAJB1 and Apg2 from the fibril (step 4). Step 4 is considered to involve structural changes in the chaperone complex, eliciting a power stroke that liberates α-Syn molecules from the internal sites and ends of fibrils. Iterative cycles of fibril binding and release successively introduce nicks into protofilaments and protofibrils, progressively disintegrating fibrils until these breaks apart (fragmentation). This process increasingly generates free fibril ends which are preferred sites for depolymerisation, liberating monomeric α-Syn.

References

Andreasson, C., Fiaux, J., Rampelt, H., Mayer, M.P., and Bukau, B. (2008). Hsp110 is a nucleotide-activated exchange factor for Hsp70. J Biol Chem *283*, 8877-8884.

Beckett, D., Kovaleva, E., and Schatz, P.J. (1999). A minimal peptide substrate in biotin holoenzyme synthetase-catalyzed biotinylation. Protein Sci *8*, 921-929.

Bieschke, J., Cohen, E., Murray, A., Dillin, A., and Kelly, J.W. (2009). A kinetic assessment of the C. elegans amyloid disaggregation activity enables uncoupling of disassembly and proteolysis. Protein Sci *18*, 2231-2241.

Bieschke, J., Russ, J., Friedrich, R.P., Ehrnhoefer, D.E., Wobst, H., Neugebauer, K., and Wanker, E.E. (2010). EGCG remodels mature alpha-synuclein and amyloid-beta fibrils and reduces cellular toxicity. Proc Natl Acad Sci U S A *107*, 7710-7715.

Blennow, K., de Leon, M.J., and Zetterberg, H. (2006). Alzheimer's disease. Lancet *368*, 387-403.

Brenner, S. (1974). The genetics of Caenorhabditis elegans. Genetics *77*, 71-94.

Bukau, B., and Horwich, A.L. (1998). The Hsp70 and Hsp60 chaperone machines. Cell *92*, 351-366.

Cantuti-Castelvetri, I., Klucken, J., Ingelsson, M., Ramasamy, K., McLean, P.J., Frosch, M.P., Hyman, B.T., and Standaert, D.G. (2005). Alpha-synuclein and chaperones in dementia with Lewy bodies. Journal of neuropathology and experimental neurology *64*, 1058-1066.

Caughey, B., and Lansbury, P.T. (2003). Protofibrils, pores, fibrils, and neurodegeneration: separating the responsible protein aggregates from the innocent bystanders. Annual review of neuroscience *26*, 267-298.

Chen, B., Retzlaff, M., Roos, T., and Frydman, J. (2011). Cellular strategies of protein quality control. Cold Spring Harbor perspectives in biology *3*, a004374.

Conway, K.A., Harper, J.D., and Lansbury, P.T. (1998). Accelerated in vitro fibril formation by a mutant alpha-synuclein linked to early-onset Parkinson disease. Nat Med *4*, 1318-1320.

Conway, K.A., Harper, J.D., and Lansbury, P.T., Jr. (2000). Fibrils formed in vitro from alpha-synuclein and two mutant forms linked to Parkinson's disease are typical amyloid. Biochemistry *39*, 2552-2563.

Danzer, K.M., Haasen, D., Karow, A.R., Moussaud, S., Habeck, M., Giese, A., Kretzschmar, H., Hengerer, B., and Kostka, M. (2007). Different species of alpha-synuclein oligomers induce calcium influx and seeding. The Journal of neuroscience : the official journal of the Society for Neuroscience *27*, 9220-9232.

Dedmon, M.M., Christodoulou, J., Wilson, M.R., and Dobson, C.M. (2005). Heat shock protein 70 inhibits alpha-synuclein fibril formation via preferential binding to prefibrillar species. The Journal of biological chemistry *280*, 14733-14740.

Dragovic, Z., Broadley, S.A., Shomura, Y., Bracher, A., and Hartl, F.U. (2006). Molecular chaperones of the Hsp110 family act as nucleotide exchange factors of Hsp70s. The EMBO journal *25*, 2519-2528.

Duennwald, M.L., Echeverria, A., and Shorter, J. (2012). Small heat shock proteins potentiate amyloid dissolution by protein disaggregases from yeast and humans. PLoS biology *10*, e1001346.

Evans, C.G., Wisen, S., and Gestwicki, J.E. (2006). Heat shock proteins 70 and 90 inhibit early stages of amyloid beta-(1-42) aggregation in vitro. The Journal of biological chemistry *281*, 33182-33191.

Finka, A., and Goloubinoff, P. (2013). Proteomic data from human cell cultures refine mechanisms of chaperone-mediated protein homeostasis. Cell Stress Chaperones *18*, 591-605.
Graf, C., Stankiewicz, M., Kramer, G., and Mayer, M.P. (2009). Spatially and kinetically resolved changes in the conformational dynamics of the Hsp90 chaperone machine. The EMBO journal *28*, 602-613.
Haass, C., and Selkoe, D.J. (2007). Soluble protein oligomers in neurodegeneration: lessons from the Alzheimer's amyloid beta-peptide. Nat Rev Mol Cell Biol *8*, 101-112.
Helsen, C.W., and Glover, J.R. (2012). Insight into molecular basis of curing of [PSI+] prion by overexpression of 104-kDa heat shock protein (Hsp104). The Journal of biological chemistry *287*, 542-556.
Higurashi, T., Hines, J.K., Sahi, C., Aron, R., and Craig, E.A. (2008). Specificity of the J-protein Sis1 in the propagation of 3 yeast prions. Proc Natl Acad Sci U S A *105*, 16596-16601.
Huang, C., Cheng, H., Hao, S., Zhou, H., Zhang, X., Gao, J., Sun, Q.H., Hu, H., and Wang, C.C. (2006). Heat shock protein 70 inhibits alpha-synuclein fibril formation via interactions with diverse intermediates. J Mol Biol *364*, 323-336.
Inoue, Y., and Yoshida, M. (2006). In vitro assay for fragmentation of amyloid fibers of yeast prion protein. Methods *39*, 56-60.
Jarrett, J.T., and Lansbury, P.T., Jr. (1993). Seeding "one-dimensional crystallization" of amyloid: a pathogenic mechanism in Alzheimer's disease and scrapie? Cell *73*, 1055-1058.
Karpinar, D.P., Balija, M.B., Kugler, S., Opazo, F., Rezaei-Ghaleh, N., Wender, N., Kim, H.Y., Taschenberger, G., Falkenburger, B.H., Heise, H.*, et al.* (2009). Pre-fibrillar alpha-synuclein variants with impaired beta-structure increase neurotoxicity in Parkinson's disease models. The EMBO journal *28*, 3256-3268.
Khurana, R., Ionescu-Zanetti, C., Pope, M., Li, J., Nielson, L., Ramirez-Alvarado, M., Regan, L., Fink, A.L., and Carter, S.A. (2003). A general model for amyloid fibril assembly based on morphological studies using atomic force microscopy. Biophysical journal *85*, 1135-1144.
Kieran, D., Kalmar, B., Dick, J.R., Riddoch-Contreras, J., Burnstock, G., and Greensmith, L. (2004). Treatment with arimoclomol, a coinducer of heat shock proteins, delays disease progression in ALS mice. Nat Med *10*, 402-405.
Kim, Y.E., Hipp, M.S., Bracher, A., Hayer-Hartl, M., and Hartl, F.U. (2013). Molecular chaperone functions in protein folding and proteostasis. Annual review of biochemistry *82*, 323-355.
Kityk, R., Kopp, J., Sinning, I., and Mayer, M.P. (2012). Structure and dynamics of the ATP-bound open conformation of Hsp70 chaperones. Mol Cell *48*, 863-874.
Knowles, T.P., Vendruscolo, M., and Dobson, C.M. (2014). The amyloid state and its association with protein misfolding diseases. Nat Rev Mol Cell Biol *15*, 384-396.
Kremer, J.R., Mastronarde, D.N., and McIntosh, J.R. (1996). Computer visualization of three-dimensional image data using IMOD. Journal of structural biology *116*, 71-76.
Labbadia, J., and Morimoto, R.I. (2015). The Biology of Proteostasis in Aging and Disease. Annual review of biochemistry.
Lee, S., Carson, K., Rice-Ficht, A., and Good, T. (2005). Hsp20, a novel alpha-crystallin, prevents Abeta fibril formation and toxicity. Protein Sci *14*, 593-601.

Lomakin, A., Chung, D.S., Benedek, G.B., Kirschner, D.A., and Teplow, D.B. (1996). On the nucleation and growth of amyloid beta-protein fibrils: detection of nuclei and quantitation of rate constants. Proc Natl Acad Sci U S A *93*, 1125-1129.
Mastronarde, D.N. (2005). Automated electron microscope tomography using robust prediction of specimen movements. Journal of structural biology *152*, 36-51.
Mattoo, R.U., Sharma, S.K., Priya, S., Finka, A., and Goloubinoff, P. (2013). Hsp110 is a bona fide chaperone using ATP to unfold stable misfolded polypeptides and reciprocally collaborate with Hsp70 to solubilize protein aggregates. The Journal of biological chemistry *288*, 21399-21411.
Mayer, M.P. (2013). Hsp70 chaperone dynamics and molecular mechanism. Trends Biochem Sci *38*, 507-514.
Muchowski, P.J., and Wacker, J.L. (2005). Modulation of neurodegeneration by molecular chaperones. Nat Rev Neurosci *6*, 11-22.
Murray, A.N., Palhano, F.L., Bieschke, J., and Kelly, J.W. (2013). Surface adsorption considerations when working with amyloid fibrils in multiwell plates and Eppendorf tubes. Protein Sci *22*, 1531-1541.
Murray, A.N., Solomon, J.P., Wang, Y.J., Balch, W.E., and Kelly, J.W. (2010). Discovery and characterization of a mammalian amyloid disaggregation activity. Protein Sci *19*, 836-846.
Nollen, E.A., Brunsting, J.F., Song, J., Kampinga, H.H., and Morimoto, R.I. (2000). Bag1 functions in vivo as a negative regulator of Hsp70 chaperone activity. Molecular and cellular biology *20*, 1083-1088.
Pemberton, S., Madiona, K., Pieri, L., Kabani, M., Bousset, L., and Melki, R. (2011). Hsc70 protein interaction with soluble and fibrillar alpha-synuclein. The Journal of biological chemistry *286*, 34690-34699.
Pieri, L., Madiona, K., Bousset, L., and Melki, R. (2012). Fibrillar alpha-synuclein and huntingtin exon 1 assemblies are toxic to the cells. Biophysical journal *102*, 2894-2905.
Pierpaoli, E.V., Gisler, S.M., and Christen, P. (1998). Sequence-specific rates of interaction of target peptides with the molecular chaperones DnaK and DnaJ. Biochemistry *37*, 16741-16748.
Rampelt, H., Kirstein-Miles, J., Nillegoda, N.B., Chi, K., Scholz, S.R., Morimoto, R.I., and Bukau, B. (2012). Metazoan Hsp70 machines use Hsp110 to power protein disaggregation. The EMBO journal *31*, 4221-4235.
Reidy, M., Miot, M., and Masison, D.C. (2012). Prokaryotic chaperones support yeast prions and thermotolerance and define disaggregation machinery interactions. Genetics *192*, 185-193.
Rutkowska, A., Mayer, M.P., Hoffmann, A., Merz, F., Zachmann-Brand, B., Schaffitzel, C., Ban, N., Deuerling, E., and Bukau, B. (2008). Dynamics of trigger factor interaction with translating ribosomes. The Journal of biological chemistry *283*, 4124-4132.
Shorter, J. (2011). The mammalian disaggregase machinery: Hsp110 synergizes with Hsp70 and Hsp40 to catalyze protein disaggregation and reactivation in a cell-free system. PLoS One *6*, e26319.
Shorter, J., and Lindquist, S. (2004). Hsp104 catalyzes formation and elimination of self-replicating Sup35 prion conformers. Science *304*, 1793-1797.
Shorter, J., and Lindquist, S. (2006). Destruction or potentiation of different prions catalyzed by similar Hsp104 remodeling activities. Mol Cell *23*, 425-438.

Spence, M.T.Z., and Johnson, I.D. (2010). The molecular probes handbook : a guide to fluorescent probes and labeling technologies, 11th edn (Carlsbad, CA: Live Technologies Corporation).
Takeuchi, H., Kobayashi, Y., Yoshihara, T., Niwa, J., Doyu, M., Ohtsuka, K., and Sobue, G. (2002). Hsp70 and Hsp40 improve neurite outgrowth and suppress intracytoplasmic aggregate formation in cultured neuronal cells expressing mutant SOD1. Brain research *949*, 11-22.
Tsai, J., and Douglas, M.G. (1996). A conserved HPD sequence of the J-domain is necessary for YDJ1 stimulation of Hsp70 ATPase activity at a site distinct from substrate binding. The Journal of biological chemistry *271*, 9347-9354.
Tsigelny, I.F., Crews, L., Desplats, P., Shaked, G.M., Sharikov, Y., Mizuno, H., Spencer, B., Rockenstein, E., Trejo, M., Platoshyn, O.*, et al.* (2008). Mechanisms of hybrid oligomer formation in the pathogenesis of combined Alzheimer's and Parkinson's diseases. PLoS One *3*, e3135.
Tuite, M.F., Marchante, R., and Kushnirov, V. (2011). Fungal prions: structure, function and propagation. Topics in current chemistry *305*, 257-298.
Tzankov, S., Wong, M.J., Shi, K., Nassif, C., and Young, J.C. (2008). Functional divergence between co-chaperones of Hsc70. The Journal of biological chemistry *283*, 27100-27109.
Uversky, V.N., Li, J., and Fink, A.L. (2001). Evidence for a partially folded intermediate in alpha-synuclein fibril formation. The Journal of biological chemistry *276*, 10737-10744.
van Ham, T.J., Thijssen, K.L., Breitling, R., Hofstra, R.M., Plasterk, R.H., and Nollen, E.A. (2008). C. elegans model identifies genetic modifiers of alpha-synuclein inclusion formation during aging. PLoS genetics *4*, e1000027.
Vilar, M., Chou, H.T., Luhrs, T., Maji, S.K., Riek-Loher, D., Verel, R., Manning, G., Stahlberg, H., and Riek, R. (2008). The fold of alpha-synuclein fibrils. Proc Natl Acad Sci U S A *105*, 8637-8642.
Wang, J., Farr, G.W., Zeiss, C.J., Rodriguez-Gil, D.J., Wilson, J.H., Furtak, K., Rutkowski, D.T., Kaufman, R.J., Ruse, C.I., Yates, J.R., 3rd*, et al.* (2009). Progressive aggregation despite chaperone associations of a mutant SOD1-YFP in transgenic mice that develop ALS. Proc Natl Acad Sci U S A *106*, 1392-1397.
Winkler, J., Tyedmers, J., Bukau, B., and Mogk, A. (2012). Hsp70 targets Hsp100 chaperones to substrates for protein disaggregation and prion fragmentation. The Journal of cell biology *198*, 387-404.
Winner, B., Jappelli, R., Maji, S.K., Desplats, P.A., Boyer, L., Aigner, S., Hetzer, C., Loher, T., Vilar, M., Campioni, S.*, et al.* (2011). In vivo demonstration that alpha-synuclein oligomers are toxic. Proc Natl Acad Sci U S A *108*, 4194-4199.

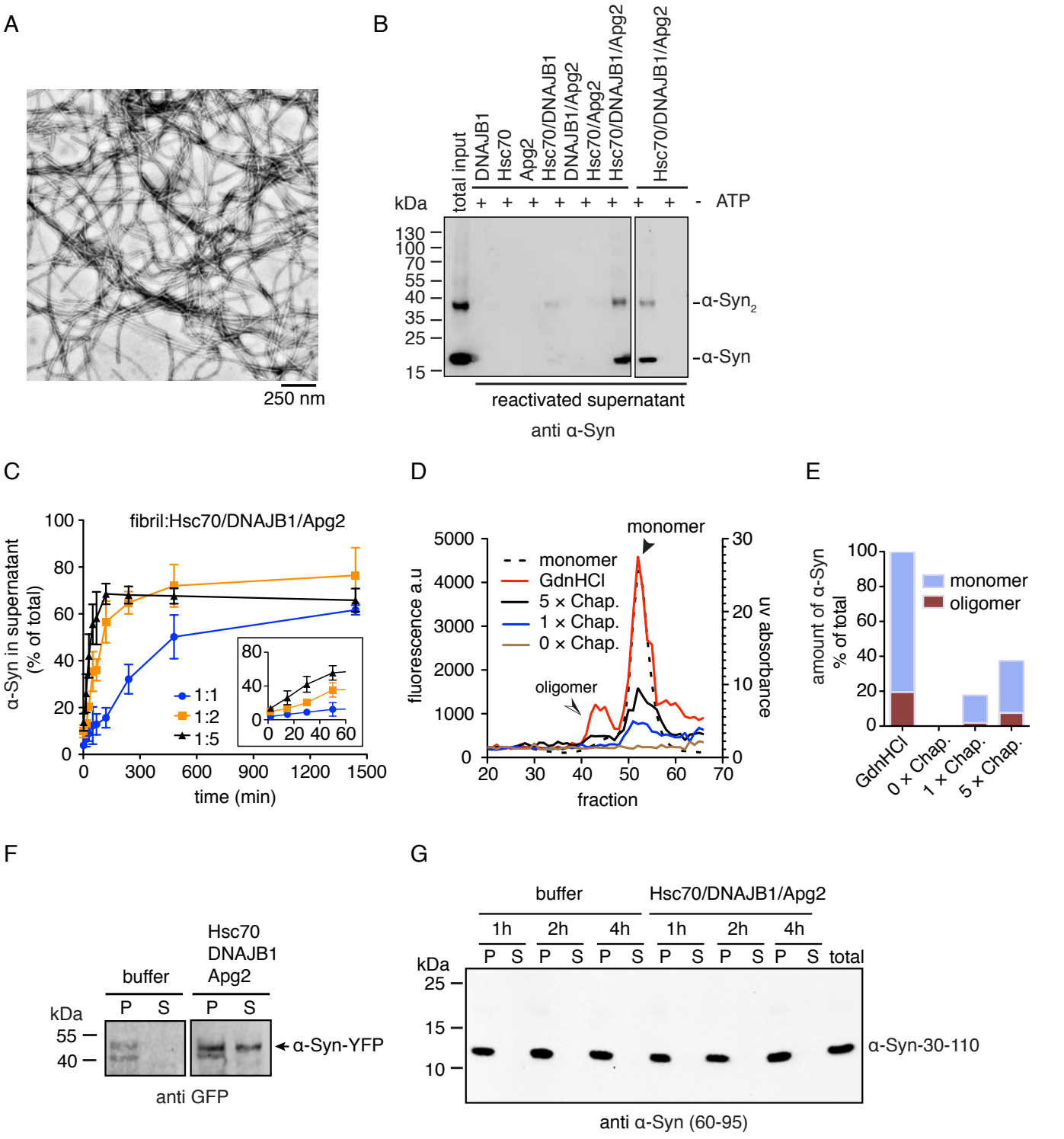
A
250 nm
B
total input
DNAJB1
Hsc70
Apg2
Hsc70/DNAJB1
DNAJB1/Apg2
Hsc70/Apg2
Hsc70/DNAJB1/Apg2
Hsc70/DNAJB1/Apg2
kDa
+ + + + + + + + - ATP
130
100
70
55
40
35
25
15
-α-Syn2
-α-Syn
reactivated supernatant
anti α-Syn
C
fibril:Hsc70/DNAJB1/Apg2
α-Syn in supernatant (% of total)
1:1
1:2
1:5
time (min)
D
monomer
GdnHCl
5 × Chap.
1 × Chap.
0 × Chap.
oligomer
fluorescence a.u
uv absorbance
fraction
E
amount of α-Syn % of total
monomer
oligomer
GdnHCl
0 × Chap.
1 × Chap.
5 × Chap.
F
buffer
Hsc70
DNAJB1
Apg2
P S P S
kDa
55
40
α-Syn-YFP
anti GFP
G
buffer
Hsc70/DNAJB1/Apg2
1h 2h 4h 1h 2h 4h
P S P S P S P S P S P S total
kDa
25
15
10
α-Syn-30-110
anti α-Syn (60-95)

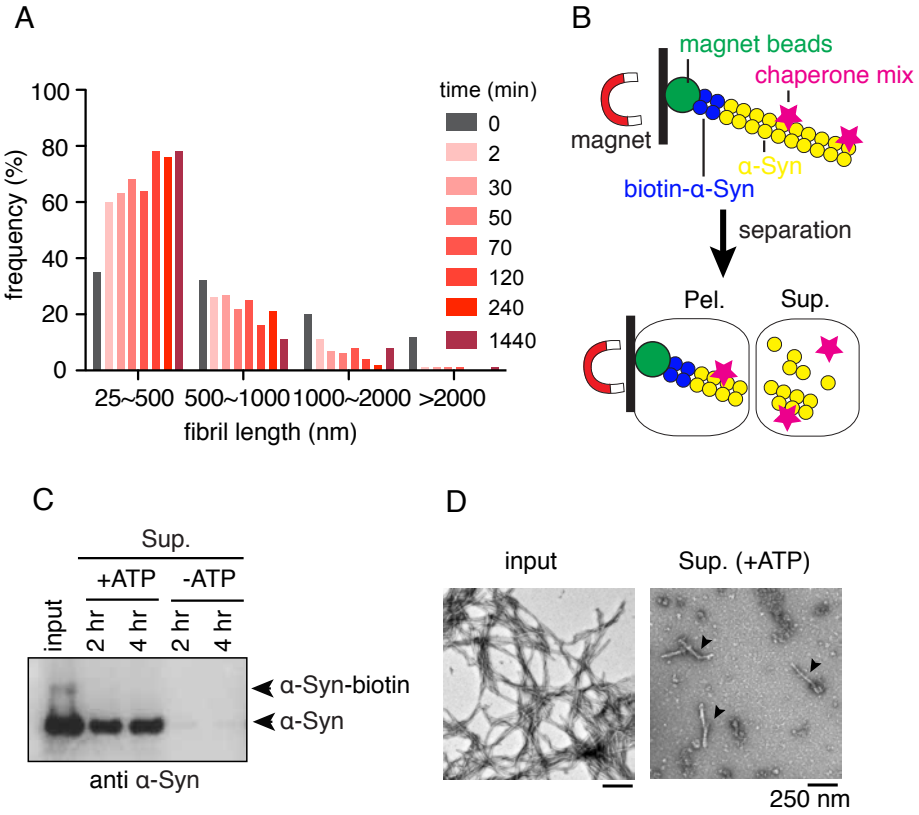

Gao et.al_Figure.2

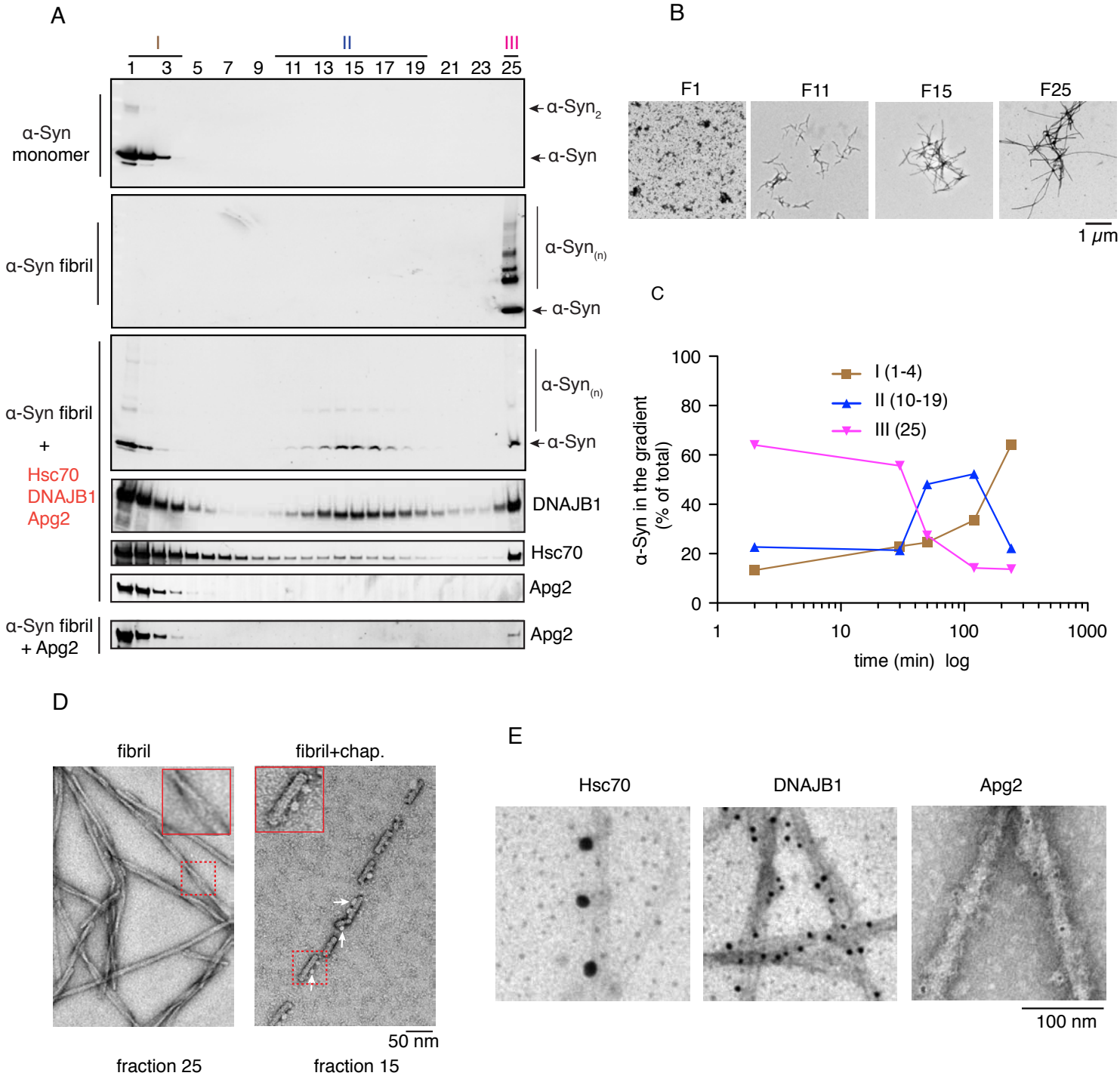

Gao et.al_Figure.3

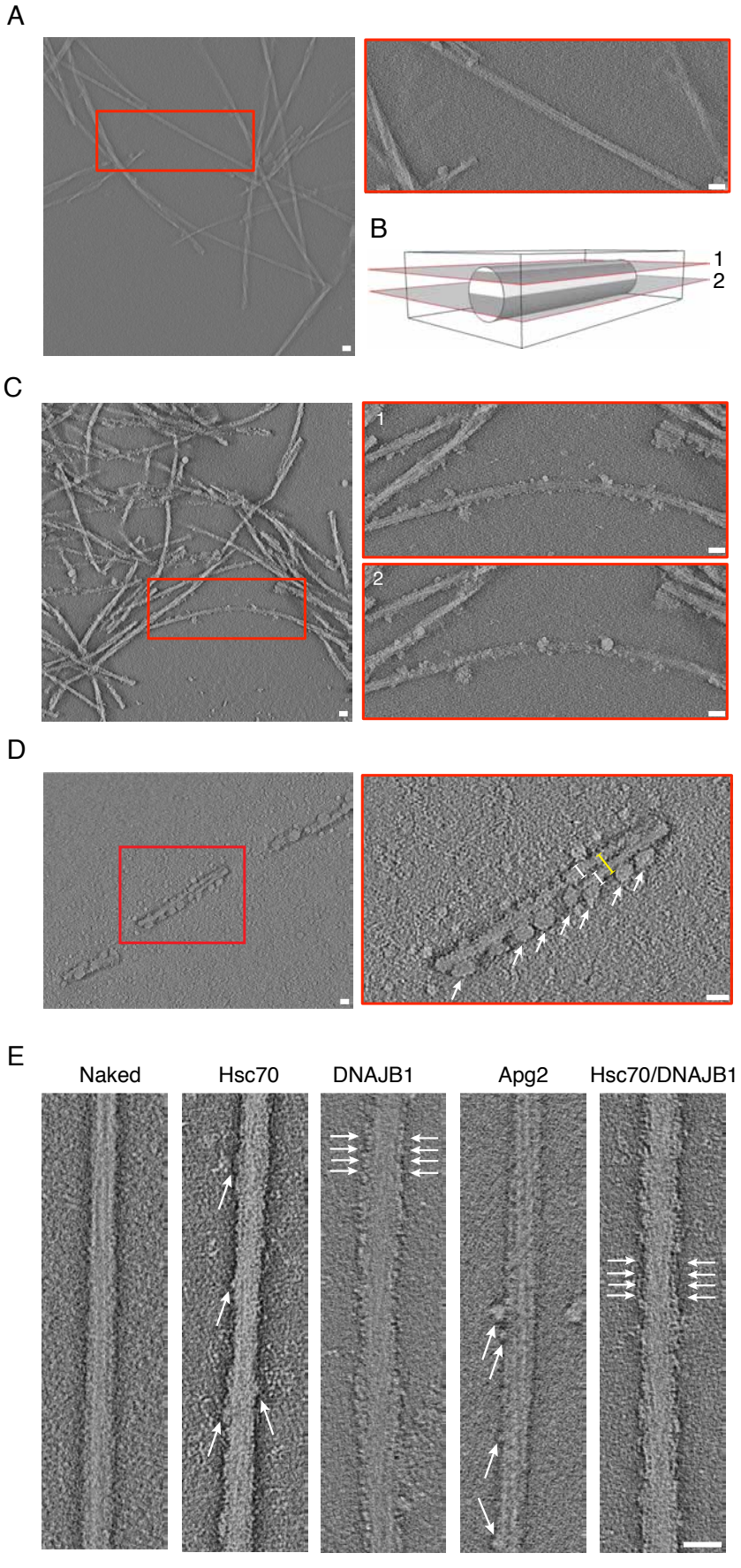

Gao et.al_Figure.4

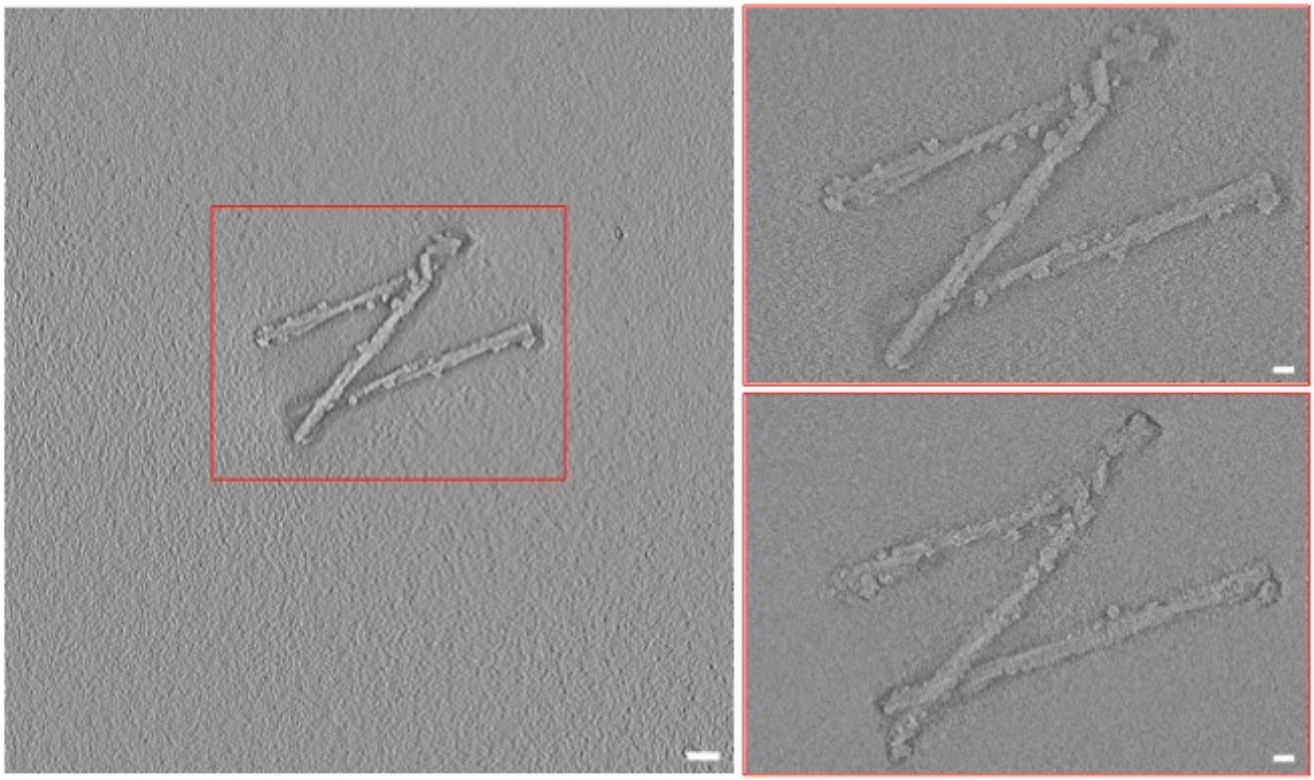

Scale bars are all 20 nm

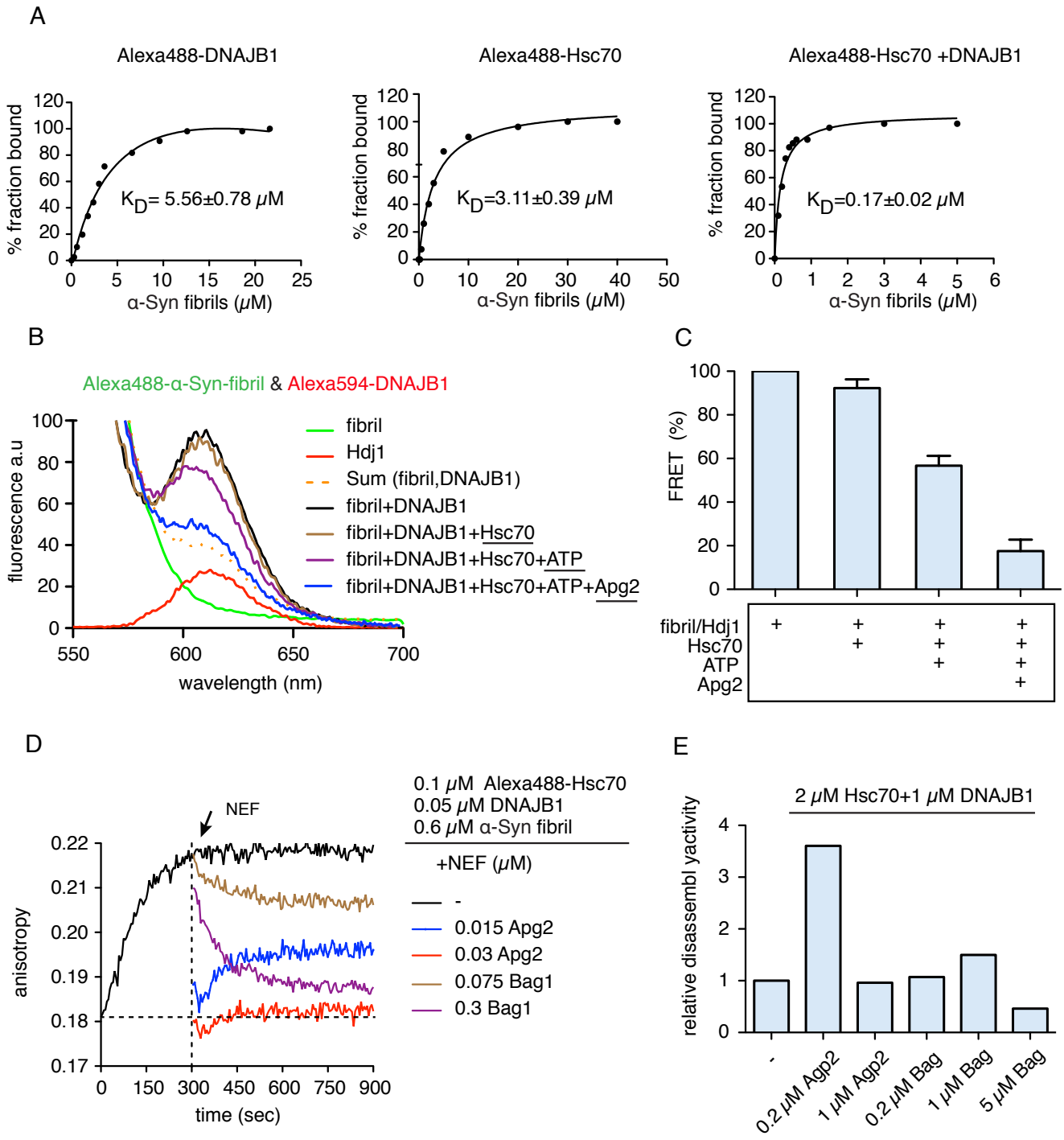

Gao et.al_Figure.5

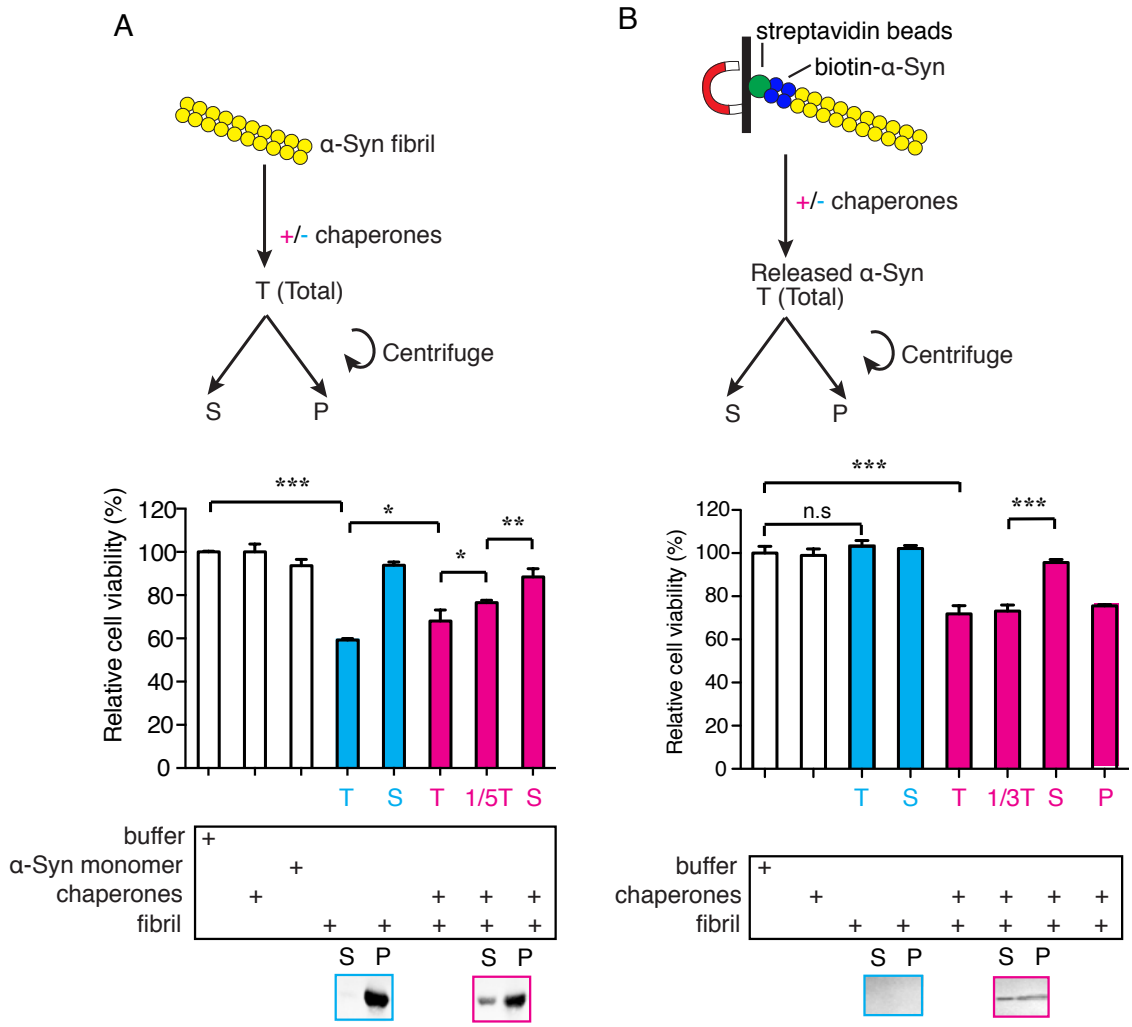

Gao et.al_Figure.6

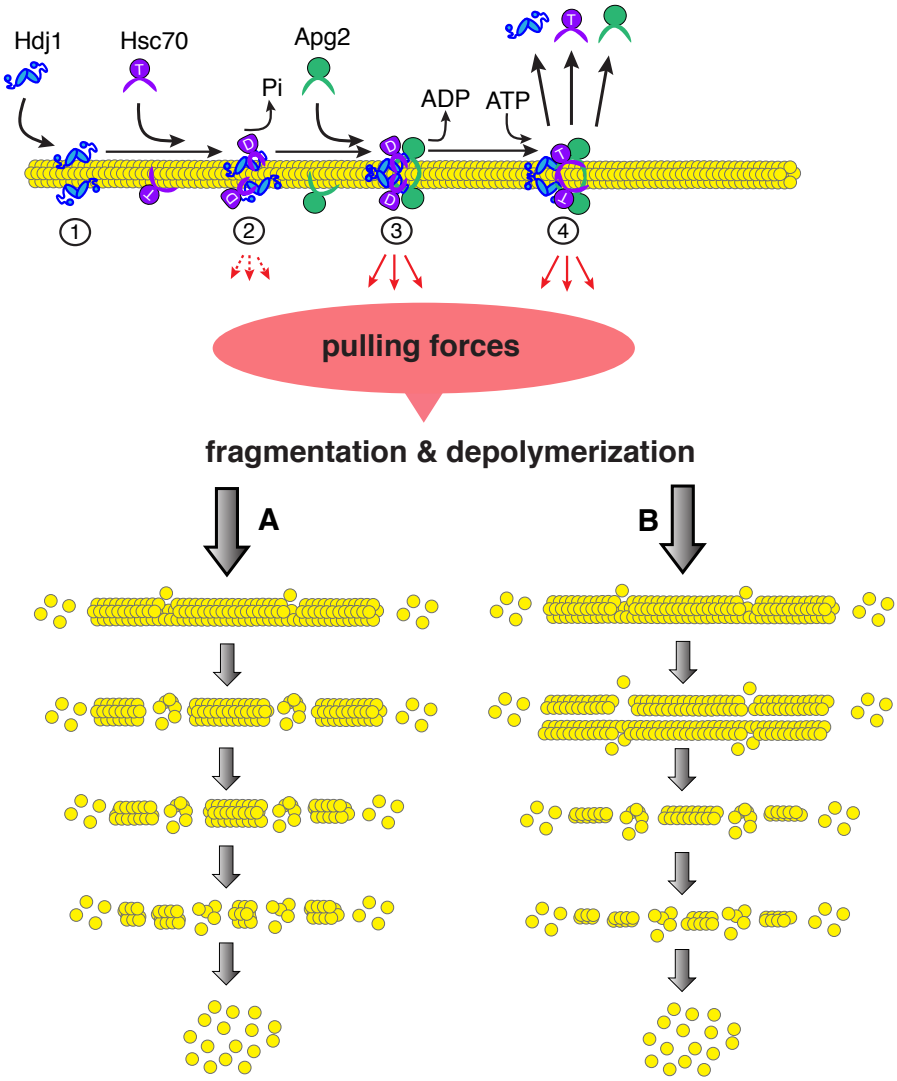

Gao et.al_Figure.7

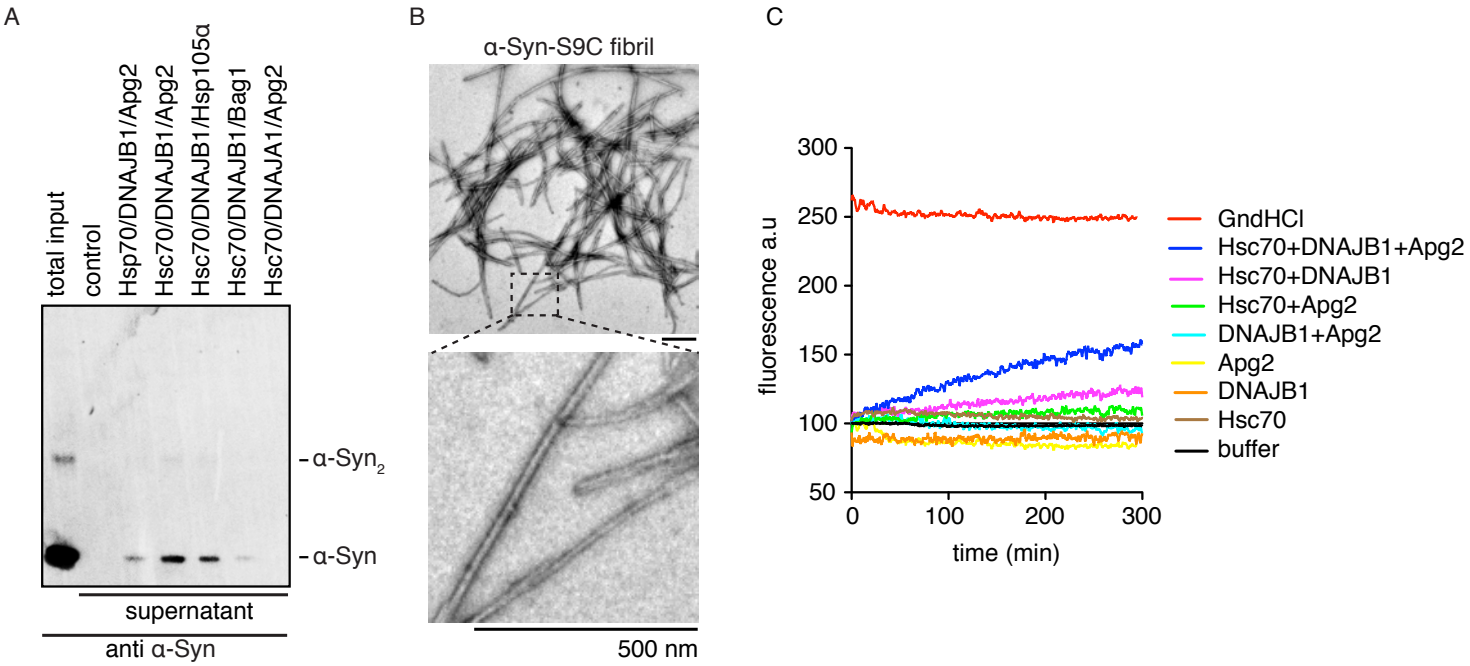

Gao et.al_Figure.S1 (to Figure 1)

A

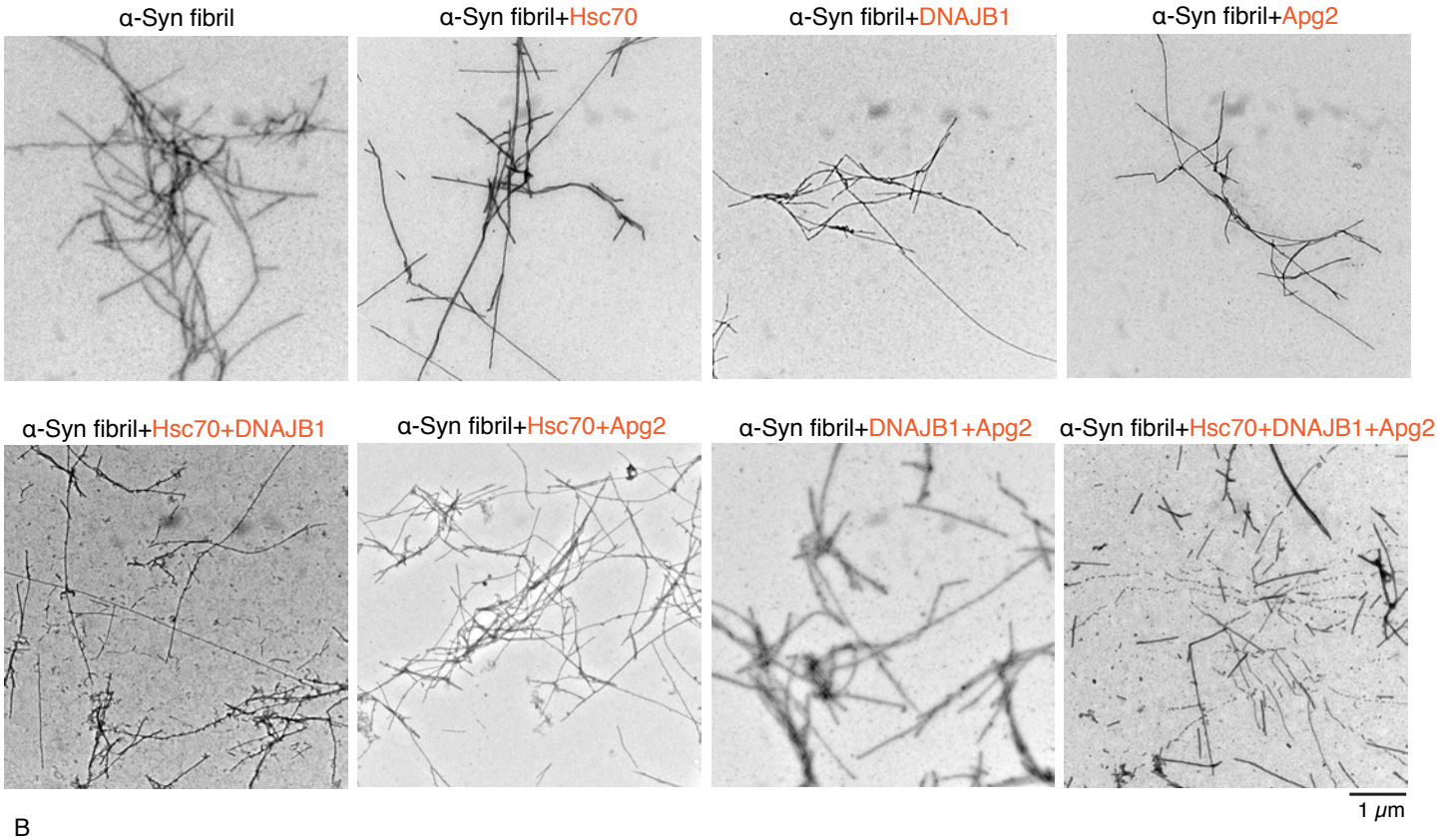

B

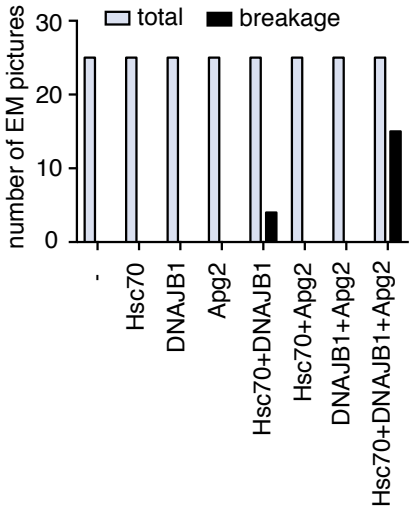

Gao et.al_Figure.S2 (to Figure 2A)

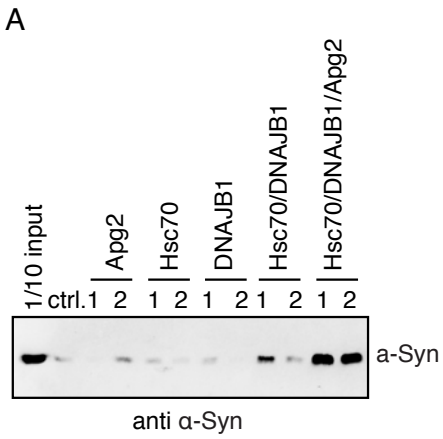

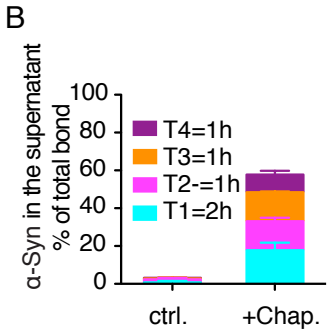

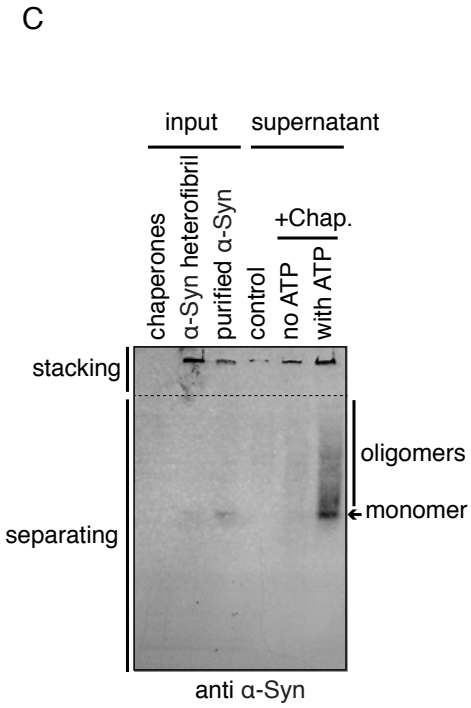

Gao et.al_Figure. S3 (to Figure. 2D)

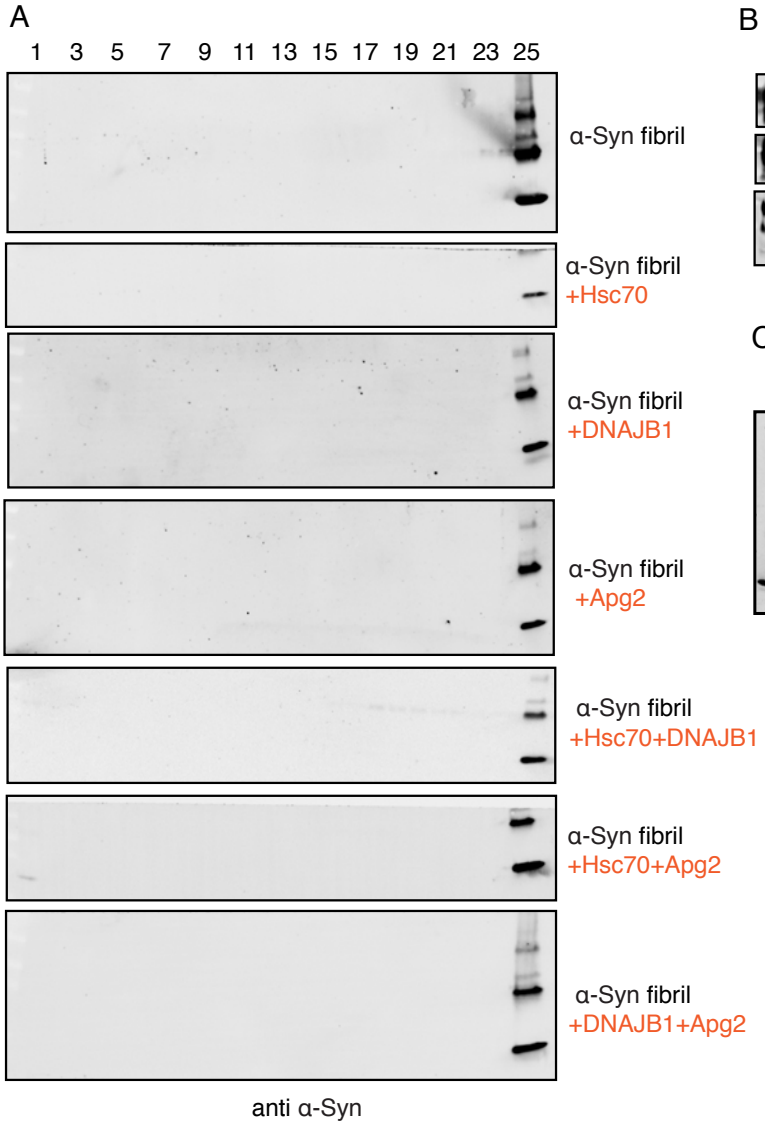

D

Probability Legend:
over 95%
80% to 94%
50% to 79%
20% to 49%
0% to 19%

#	Visible?	Starred?	MS/MS View: Identified Proteins (19)	Accession Number	Molecular Weight	Protein Grouping Ambiguity	14-223 01-03 E-14-223-01	E-14-223-02	E-14-223-03
1	✓		Heat shock cognate 71 kDa protein OS=Homo sapiens GN=HSPA8 PE=1 SV=1	HSP7C_HU...	71 kDa	★	19	21	39
2	✓		Keratin, type II cytoskeletal 1 OS=Homo sapiens GN=KRT1 PE=1 SV=6	K2C1_HUM...	66 kDa	★	17	12	17
3	✓		Keratin, type I cytoskeletal 10 OS=Homo sapiens GN=KRT10 PE=1 SV=6	K1C10_HU...	59 kDa	★	11	15	19
4	✓		DnaJ homolog subfamily B member 1 OS=Homo sapiens GN=DNAJB1 PE=1 SV=4	DNJB1_HU...	38 kDa	★	8	7	23
5	✓		Keratin, type II cytoskeletal 2 epidermal OS=Homo sapiens GN=KRT2 PE=1 SV=2	K22E_HUM...	65 kDa	★	15	12	9
6	✓		Heat shock 70 kDa protein 4 OS=Homo sapiens GN=HSPA4 PE=1 SV=4	HSP74_HU...	94 kDa		3	14	9
7	✓		Alpha-synuclein OS=Homo sapiens GN=SNCA PE=1 SV=1	SYUA_HUM...	14 kDa		5	4	6
8	✓		Keratin, type I cytoskeletal 9 OS=Homo sapiens GN=KRT9 PE=1 SV=3	K1C9_HUM...	62 kDa	★	5	2	5
9	✓		Serum albumin OS=Homo sapiens GN=ALB PE=1 SV=2	ALBU_HUM...	69 kDa		3	2	2
10	✓		Keratin, type I cytoskeletal 16 OS=Homo sapiens GN=KRT16 PE=1 SV=4	K1C16_HU...	51 kDa	★	6	0	1
11	✓		Keratin, type II cytoskeletal 6C OS=Homo sapiens GN=KRT6C PE=1 SV=3	K2C6C_HU...	60 kDa	★	8		

Gao et.al_Figure.S4 (to Figure. 3A)

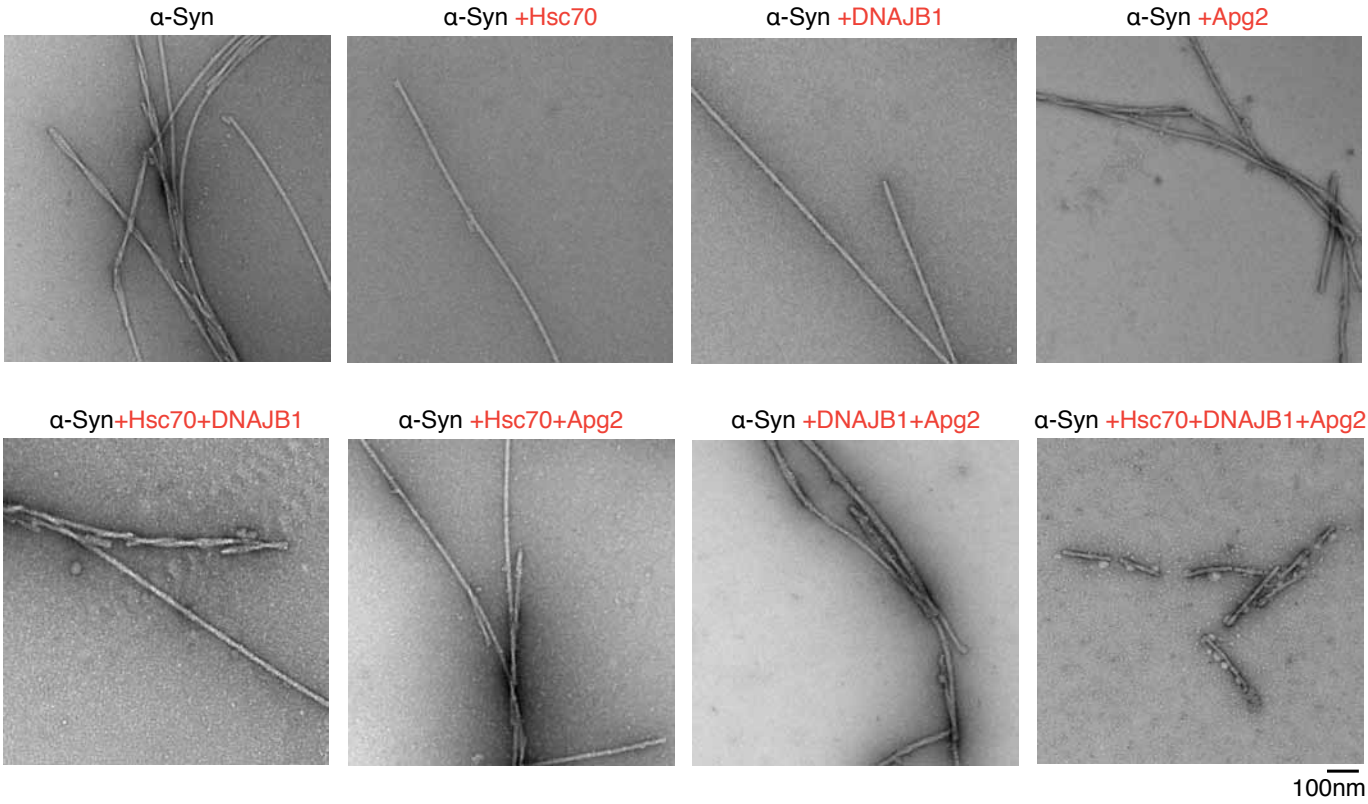

all these are samples from fraction 25.

Gao et.al_Figure.S5 (to Figure. 3D)

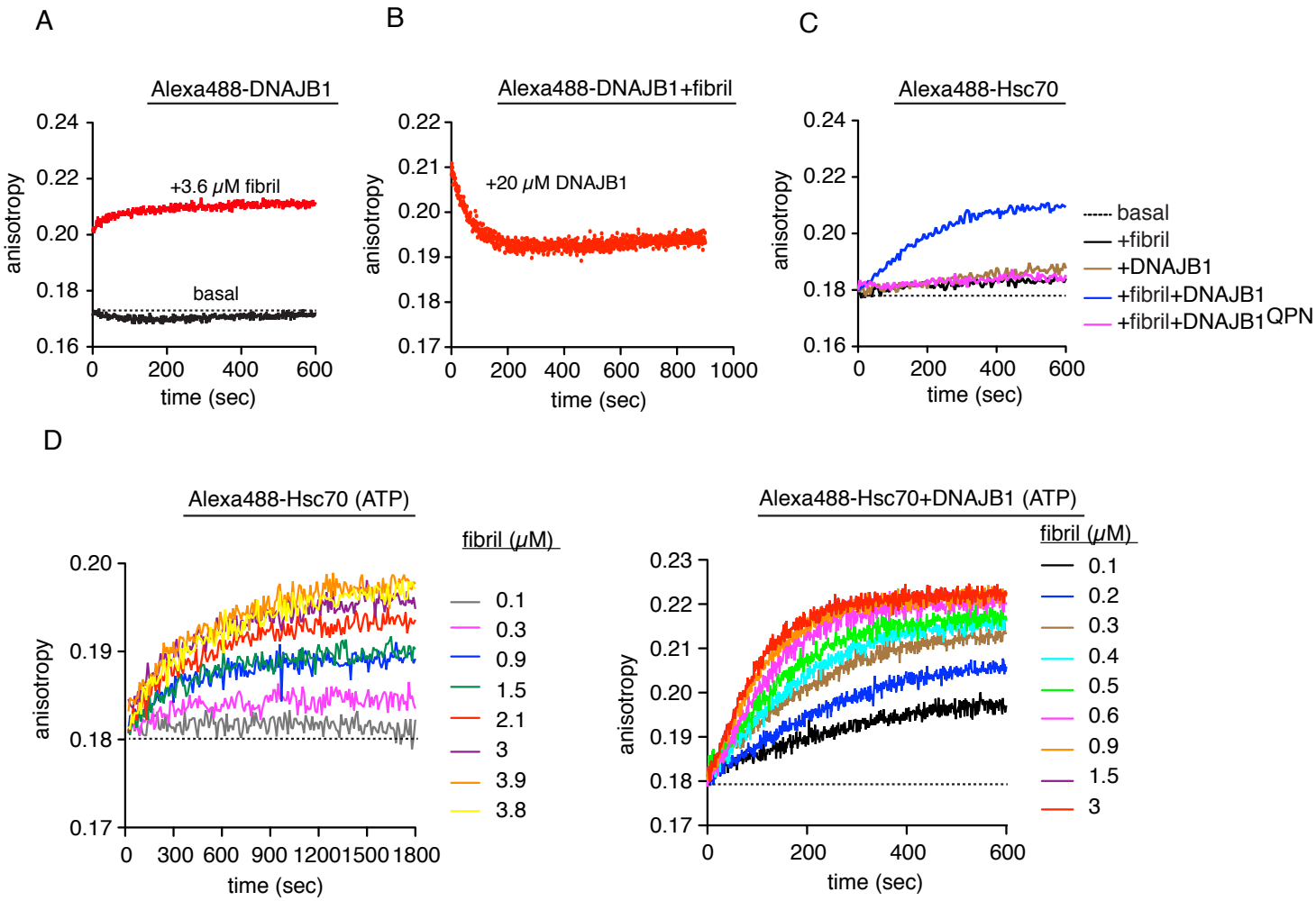

Gao et.al_Figure.S6 (to Figure. 5B)

A

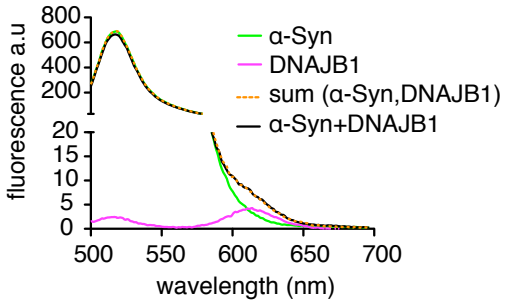

B

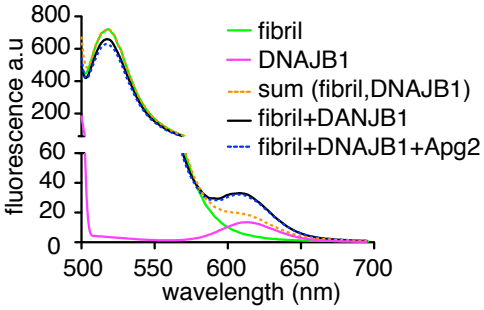

Gao et.al_Figure.S7 (to Figure. 5C)

A

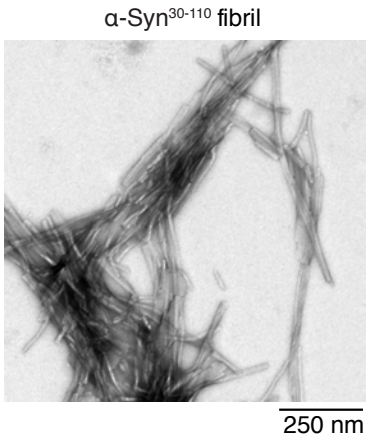
α-Syn30-110 fibril
250 nm

B

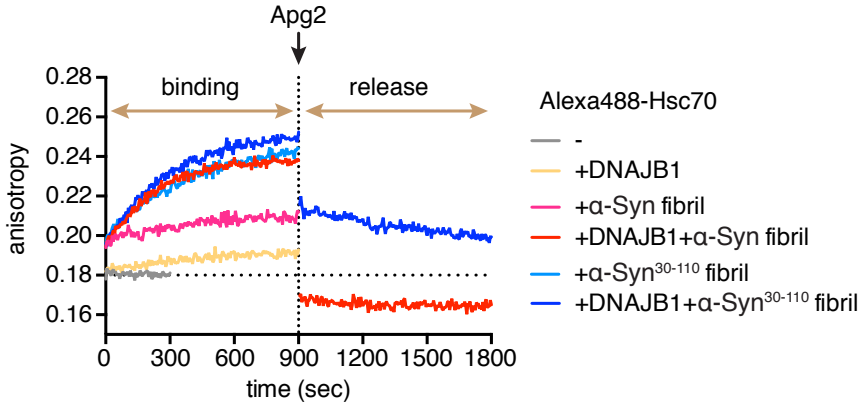
Apg2
binding
release
anisotropy
0.28
0.26
0.24
0.22
0.20
0.18
0.16
0
300
600
900
1200
1500
1800
time (sec)
Alexa488-Hsc70
-
+DNAJB1
+α-Syn fibril
+DNAJB1+α-Syn fibril
+α-Syn30-110 fibril
+DNAJB1+α-Syn30-110 fibril

C

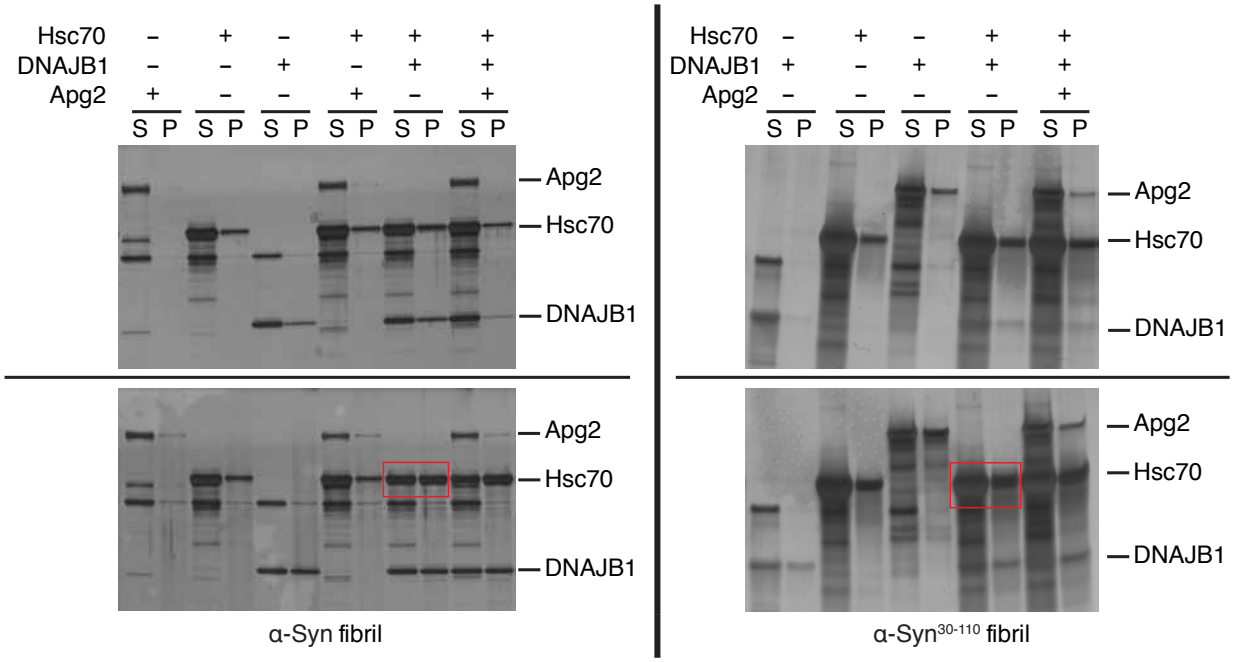
Hsc70
DNAJB1
Apg2
S P S P S P S P S P S P
Apg2
Hsc70
DNAJB1
α-Syn fibril
α-Syn30-110 fibril